2 Physics and Instrumentation in PET*

Dale L Bailey, Joel S Karp and Suleman Surti

Introduction

In 1928 Paul AM Dirac postulated that a subatomic particle existed which was equivalent in mass to an electron but carried a positive charge. Carl Anderson experimentally observed these particles, which he called *positrons*, in cosmic ray research using cloud chambers in 1932. Both received Nobel Prizes in physics for their contributions. The positrons observed by Anderson were produced naturally in the upper atmosphere by the conversion of high-energy cosmic radiation into an electron–positron pair. Soon after this it was shown that when positrons interact with matter they give rise to two photons which, in general, are emitted simultaneously in almost exactly opposed directions. This sequence of events touches on many of the momentous developments in physics that occurred in the first 50 years of the twentieth century: radioactivity, Einstein's special relativity (energy–mass equivalence famously described by $E = mc^2$), quantum mechanics, de Broglie's wave–particle duality, and the laws of conservation of physical properties.

Today we produce positron-emitting radionuclides under controlled laboratory conditions in particle accelerators in the hospital setting for use in positron emission tomography (PET). In this chapter we will examine the basic physics of radioactivity and positrons and their detection as it relates to PET.

Models of the Atom

We use models, or representations, constantly in our lives. A painting, for example, is one individual's representation of a particular scene or feeling. It is clearly not the scene itself, but it is a model, or an attempt, to capture some expression of the reality as perceived by the artist. Likewise, scientists use models to describe various concepts about very-large-scale phenomena such as the universe, and very-small-scale phenomena such as the constituent components of all matter. One important feature of a model is that it usually has a restricted range over which it applies. Thus, we employ different models to account for different observations of the same entity, the classical example being the wave–particle duality of radiation: sometimes it is convenient to picture radiation as small discrete "packets" of energy that we can count individually, and at other times radiation appears to behave like a continuous entity or wave. The latter is evidenced by phenomena such as the diffraction of coherent light sources in a double-slit experiment. This could present a problem if we were to confuse the model and reality, but we emphasize again that the model is a *representation* of the underlying reality that we observe.

Amongst the ancient Greeks, Aristotle favored a continuous matter model composed of air, earth, fire, and water, where one could go on dividing matter infinitely into smaller and smaller portions. Others, though, such as Democritus, preferred a model in which matter was

* Chapter reproduced from Valk PE, Bailey DL, Townsend DW, Maisey MN. Positron Emission Tomography: Basic Science and Clinical Practice. Springer-Verlag London Ltd 2003, 41–67.

corpuscular. By the nineteenth century it was clear that chemicals combined in set proportions, thus supporting a corpuscular, or discrete, model of matter. At the turn of the twentieth century evidence was mounting that there were basic building blocks of matter called atoms (*Greek*: *indivisible*), but the question remained as to what, if anything, the atoms themselves were composed of. It was shown by JJ Thomson and, later, Ernest (Lord) Rutherford, that atoms could be broken down into smaller units in experiments using cathode ray tubes. Thomson proposed a model of the atom that was composed of a large, uniform and positively charged sphere with smaller negative charges embedded in it to form an electrostatically neutral mixture. His model of the atom is known as the "plum pudding" atom. Rutherford showed, however, that alpha particles (doubly ionized helium nuclei emitted from some unstable atoms such as radium) could pass through sheets of aluminum, and that this was at odds with the Thomson model. He proposed a model similar to that used to describe the orbit of the planets of the solar system about the sun (the "planetary" model). The Rutherford model had a central positive core – the nucleus – about which a cloud of electrons circulated. It predicted that most of the space in matter was unoccupied (thus allowing particles and electromagnetic radiation to pass through). The Rutherford model, however, presented a problem because classical physics predicted that the revolving electrons would emit energy, resulting in a spiralling of the electrons into the nucleus. In 1913, Bohr introduced the constraint that electrons could only orbit at certain discrete radii, or energy levels, and that in turn only a small, finite number of electrons could exist in each energy level. Most of what was required to understand the subatomic behavior of particles was now known. This is the Bohr (planetary) model of the atom. Later, the neutron was proposed by Chadwick (1932) as a large particle roughly equivalent to the mass of a proton, but without any charge, that also existed in the nucleus of the atom.

We shall continue to use the planetary model of the atom for much of our discussion. The model breaks down in the realm of quantum mechanics, where Newtonian physics and the laws of motion no longer apply, and as particles approach relativistic speeds (i.e., approaching the speed of light). Also, there are times when we must invoke a non-particulate model of the atom where the particles need to be viewed as waves (or, more correctly, *wave functions*). Electrons, for example, can be considered at times to be waves. This helps to explain how an electron can pass through a "forbidden" zone between energy levels and appear in the next level without apparently having passed through the forbidden area, defined as a region of space where there is zero probability of the existence of an electron. It can do so if its wave function is zero in this region. For a periodic wave with positive and negative components this occurs when the wave function takes a value of zero. Likewise, electromagnetic radiation can be viewed as particulate at times and as a wave function at other times. The planetary model of the atom is composed of nucleons (protons and neutrons in the nucleus of the atom) and circulating electrons. It is now known that these particles are not the fundamental building blocks of matter but are themselves composed of smaller particles called *quarks*. A deeper understanding of the elementary particles, and the frequently peculiar world of quantum physics, is beyond the scope of this book.

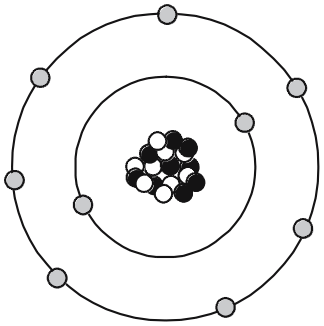

Figure 2.1. Atomic "planetary" model of radioactive fluorine-18 (^{18}F). The nucleus contains 9 protons (●) and 9 neutrons (○) and there are 9 electrons circulating in defined orbits. Stable fluorine would contain 10 neutrons.

The simple planetary model of the atom is illustrated in Fig. 2.1 for the case of radioactive fluorine-18 ($^{18}_{9}F$) . Nine orbital electrons circulate in defined energy levels about a central nucleus containing nine neutrons and nine protons. Stable fluorine is $^{19}_{9}F$ i.e., the nucleus contains one more neutron than protons and this produces a stable configuration. In all non-ionized atoms the number of electrons equals the number of protons, with the difference between the atomic number (Z) and mass number (A) being accounted for by the neutrons. In practice we usually omit the atomic number when writing radionuclide species (e.g., ^{18}F) as it is implicit in the element's symbol.

Mass and Energy

In 1900 Max Planck demonstrated that the energy (E) of electromagnetic radiation was simply related to the

frequency of the radiation (υ) by a constant (Planck's constant, h):

$$E = h\upsilon \tag{1}$$

In addition, experiments indicated that the radiation was only released in discrete "bursts". This was a startling result as it departed from the classical assumption of continuous energy to one in which electromagnetic radiation could only exist in integral multiples of the product of $h\upsilon$. The radiation was said to be *quantized*, and the discrete quanta became known as *photons*. Each photon contained an amount of energy that was an integer multiple of $h\upsilon$. The unit for energy is the joule (J), and we can calculate the energy of the radiation contained in a photon of wavelength of, for example, 450 nm as:

$$\begin{aligned} E = h\upsilon = \frac{hc}{\lambda} &= \frac{6.63 \times 10^{-34}\text{J.s} \times 3 \times 10^{8}\text{m.s}^{-1}}{450 \times 10^{-9}\text{m}} \\ &= 4.42 \times 10^{-19}\text{J} \end{aligned} \tag{2}$$

This radiation (450 nm) corresponds to the portion of the visible spectrum towards the ultraviolet end. Each photon of light at 450 nm contains the equivalent of 4.42×10^{-19} J of energy in a discrete burst. We shall see the significance of this result later in this chapter when we discuss the emission of photons from scintillators.

The joule is the Système International d'Unites (abbreviated SI) unit of energy, however, a derived unit used frequently in discussions of the energy of electromagnetic and particulate radiation is the *electron volt* (eV). The electron volt is defined as the energy acquired when a unit charge is moved through a potential difference of one volt. Energy in joules can be converted to energy in electron volts (eV) by dividing by the conversion factor 1.6×10^{-19} J.eV^{-1}. Thus, the energy in eV for photons of 450 nm would be:

$$\begin{aligned} E = 4.42 \times 10^{-19}\text{J} &\equiv \frac{4.42 \times 10^{-19}\text{J}}{1.6 \times 10^{-19}\text{J.eV}^{-1}} \\ &= 2.76\ \text{eV} \end{aligned} \tag{3}$$

X rays and gamma rays have energies of thousands to millions of electron volts per photon (Fig. 2.2).

Einstein's Special Theory of Relativity, published in 1905 while he was working in the patent office in Zurich, turned the physical sciences on its head. It predicted, amongst other things, that the speed of light was constant for all observers independent of their frame of reference (and therefore that time was no longer constant), and that mass and energy were equivalent. This means that we can talk about the *rest-mass equivalent energy* of a particle, which is the energy that would be liberated if all of the mass were to be converted to energy. By *rest mass* we mean that the particle

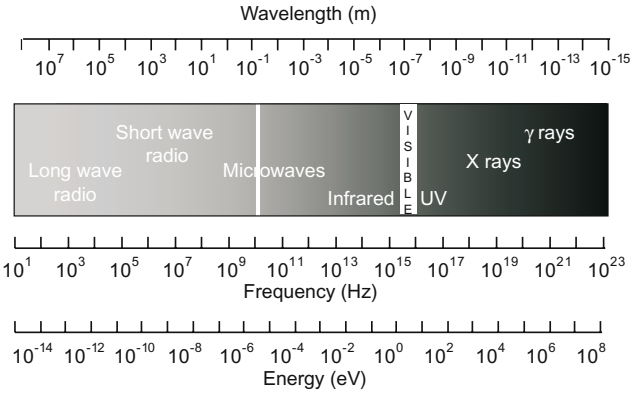

Figure 2.2. The electromagnetic spectrum showing the relationship between wavelength, frequency, and energy measured in electron volts (eV).

is considered to be at rest, i.e., it has no kinetic energy. Consider the electron, which has a rest mass of 9.11×10^{-31} kg; we can calculate the amount of energy this mass is equivalent to from:

$$\begin{aligned} E &= mc^2 \\ &= 9.11 \times 10^{-31}\text{kg} \times (3 \times 10^{8})^2\ \text{m.s}^{-1} \\ &= 8.2 \times 10^{-14}\ \text{J} \\ &\equiv \frac{8.2 \times 10^{-14}\text{J}}{1.6 \times 10^{-19}\ \text{J.eV}^{-1}} \\ &= 511\ \text{keV} \end{aligned} \tag{4}$$

The reader may recognize this as the energy of the photons emitted in positron–electron annihilation.

Conservation Laws

The principle of the conservation of fundamental properties comes from classical Newtonian physics. The concepts of conservation of mass and conservation of energy arose independently, but we now see that, because of the theory of relativity, they are merely two expressions of the same fundamental quantity. In the last 20–30 years the conservation laws have taken on slightly different interpretations from the classical ones: previously they were considered to be inviolate and equally applicable to all situations. Now, however, there are more conservation laws, and they have specific domains in which they apply as well as situations in which they break down. To classify these we must mention the four fundamental forces of nature. They are called the *gravitational*, *electromagnetic*, *strong*, and *weak* forces. It is believed that these forces are the only mechanisms which can act on the various

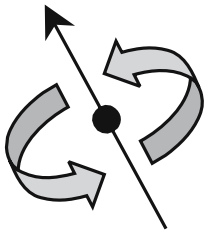

Figure 2.3. The spin quantum number for a particle can be pictured as a vector in the direction of the axis about which a particle is rotating. In this example, spin can be either "up" or "down".

properties of fundamental particles which make up all matter. These properties are electrostatic charge, energy and mass, momentum, spin and iso-spin, parity, strangeness and hypercharge (a quantity derived from strangeness and baryon numbers).

Charge is the electrostatic charge on a particle or atom and occurs in integer multiples of 1.6×10^{-19}.

Energy and *mass* conservation are well known from classical theory and are unified under special relativity.

Angular and *linear momentum* are the product of the mass (or moment of inertia) and the linear (or angular) velocity of a particle or atom.

Spin (s) and Isospin (i): Spin is the intrinsic angular momentum of a particle. It can be thought of by using the model of a ball rotating about its axis (Fig. 2.3). Associated with this rotation will be angular momentum which can take values in an arbitrary direction (labelled z) between –s to +s. The universe can be divided into two groups of particles on the basis of spin: those with spin $\frac{1}{2}$, and those with integer spin of 0, 1, or 2. The particles with spin $\frac{1}{2}$ are the mass-containing particles of the universe (fermions); the spin 0, 1, and 2 particles are the "force-carrying" particles (bosons). Some bosons, such as the pion, which serve as exchange particles for the strong nuclear force, are "virtual" particles that are very short-lived. Only spin $\frac{1}{2}$ particles are subject to the Pauli exclusion principle, which states that no two particles can have exactly the same angular momentum, spin, and other quantum mechanical physical properties. It was the concept of spin that led Dirac to suggest that the electron had an antimatter equivalent, the positron. Iso-spin is another quantum mechanical property used to describe the symmetry between different particles that behave almost identically under the influence of the strong force. In particular, the isospin relates the symmetry between a particle and its anti-particle as well as nucleons such as protons and neutrons that behave identically when subjected to the strong nuclear force. Similar to the spin, the isospin, *i*, can have half integer as well as integer values together with a special z direction which ranges in magnitude from $-i$ to $+i$. We shall see later that under certain conditions a high-energy photon (which has zero charge and isospin) can spontaneously materialize into an electron–positron pair. In this case both charge and isospin are conserved, as the electron has charge –1 and spin $+\frac{1}{2}$, and the positron has charge +1 and spin $-\frac{1}{2}$. Dirac possessed an over whelming sense of the symmetry in the universe, and this encouraged him to postulate the existence of the positron. Table 2.1 shows physical properties of some subatomic particles.

Parity is concerned with the symmetry properties of the particle. If all of the coordinates of a particle are reversed, the result may either be identical to the original particle, in which case it would be said to have *even* parity, or the mirror image of the original, in which case the parity is *odd*. Examples illustrating odd and even functions are shown in Fig. 2.4. Parity is conserved in all but weak interactions, such as beta decay.

The main interactions that we are concerned with are summarized in Table 2.2.

These are believed to be the only forces which exist in nature, and the search has been ongoing since the time of Einstein to unify these in to one all-encompassing law, often referred to as the Grand Unified Theory. To date, however, all attempts to find a grand unifying theory have been unsuccessful.

The fundamental properties and forces described here are referred to as the "Standard Model". This is the most widely accepted theory of elementary parti-

Table 2.1. Physical properties of some subatomic particles.

Particle	Symbol	Rest Mass (kg)	Charge	Spin	Isospin	Parity
Electron	e^-	9.11×10^{-31}	–1	$\frac{1}{2}$	$+\frac{1}{2}$	Even
Positron	e^+	9.11×10^{-31}	+1	$\frac{1}{2}$	$-\frac{1}{2}$	Even
Proton	p^+	1.673×10^{-27}	+1	$\frac{1}{2}$	$+\frac{1}{2}$	Even
Neutron	n^0	1.675×10^{-27}	0	$\frac{1}{2}$	$-\frac{1}{2}$	Even
Photon	Q	0	0	1	–	Odd
Neutrino	n	~0	0	$\frac{1}{2}$	$\frac{1}{2}$	Even

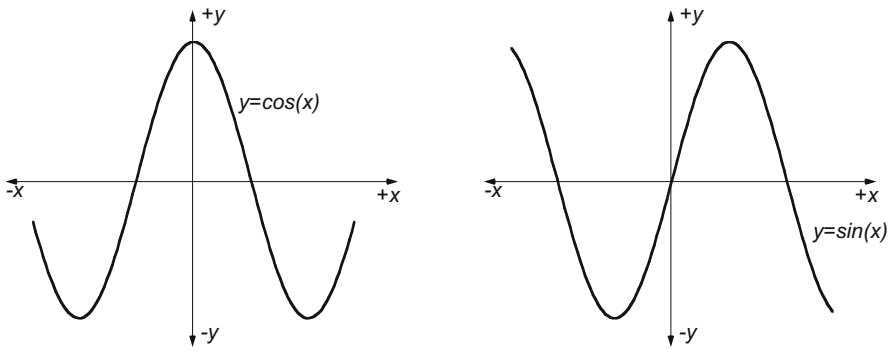

Figure 2.4. Examples of even (left) and odd (right) functions, to illustrate parity. In the even example (y = cos(x)) the positive and negative values of x have the same y-values; for the odd function (y = sin(x)) the negative x-values have opposite sign to the positive x-values.

Table 2.2. The table indicates whether the property listed is conserved under each of the fundamental interactions shown (gravity is omitted).

Property	Electromagnetic	Strong	Weak
Charge	Yes	Yes	Yes
Energy/mass	Yes	Yes	Yes
Angular momentum	Yes	Yes	Yes
Linear momentum	Yes	Yes	Yes
Iso-spin	No	Yes	No
Parity	Yes	Yes	No
Strangeness	Yes	Yes	No

cles and their interactions, which applies for all forces but gravity. The Standard Model remains a model though, and does not explain all observed phenomena, and work continues to find a grand unifying theory.

Radiation

Radiation can be classified into electromagnetic or particulate. *Ionising radiation* is radiation that has sufficient energy associated with it to remove electrons from atoms, thus causing ionisation. This is restricted to high-energy electromagnetic radiation (x and γ radiation) and charged particles (α, β^-, β^+). Examples of non-ionising electromagnetic radiation include light, radio, and microwaves. We will concern ourselves specifically with ionising radiation as this is of most interest in nuclear medicine and radiological imaging.

Electromagnetic Radiation

Electromagnetic radiation is pure energy. The amount of energy associated with each "bundle", or quantum, of energy is determined by the wavelength (λ) of the radiation. Human senses are capable of detecting some forms of electromagnetic radiation, for example, thermal radiation, or heat, ($\lambda \approx 10^{-5}$m), and visible light ($\lambda \approx 10^{-7}$m). The energy of the radiation can be absorbed to differing degrees by different materials: light can be stopped (absorbed) by paper, whereas radiation with longer wavelength (e.g., radio waves) or higher energy (γ rays) can penetrate the same paper.

We commenced our discussion at the beginning of this chapter with the comment that we are dealing with models of reality, rather than an accurate description of the reality itself; we likened this to dealing with paintings of landscapes rather than viewing the landscapes themselves. This is certainly the case when we discuss electromagnetic and particulate radiation. It had long been known that light acted like a wave, most notably because it caused interference patterns from which the wavelength of the light could be determined. Radiation was thought to emanate from its point of origin like ripples on the surface of a pond after a stone is dropped into it. This concept was not without its difficulties, most notably, the nature of the medium through which the energy was transmitted. This proposed medium was known as the "ether", and many experiments sought to produce evidence of its existence to no avail. Einstein, however, interpreted some experiments performed at the turn of the twentieth century where light shone on a photocathode could induce an electric current (known as the photoelectric effect) as showing that light acted as a particle. Einstein proposed that radiant energy was quantized into discrete packets, called *photons*. Thus, electromagnetic radiation could be viewed as having wave-like and particle-like properties. This view persists to this day and is known as the wave–particle duality. In 1924, Louis Victor, the Duc de Broglie, proposed that if wave–particle duality could apply to electromagnetic radiation, it could also apply to matter. It is now known that this is

true: electrons, for example, can exhibit particle-like properties such as when they interact like small billiard balls, or wave-like properties as when they undergo diffraction. Electrons can pass from one position in space to another, separated by a "forbidden zone" in which they cannot exist, and one way to interpret this is that the electron is a wave that has zero amplitude within the forbidden zone. The electrons could not pass through these forbidden zones if viewed strictly as particles.

An important postulate proposed by Neils Bohr was that De Broglie's principle of wave–particle duality was complementary. He stated that either the wave or the particle view can be taken to explain physical phenomena, but not both at the same time.

Electromagnetic radiation has different properties depending on the wavelength, or energy, of the quanta. Only higher-energy radiation has the ability to ionize atoms, due to the energy required to remove electrons from atoms. Electromagnetic ionising radiation is restricted to x and γ rays, which are discussed in the following sections.

X rays: X rays are electromagnetic radiation produced within an atom, but outside of the nucleus. *Characteristic* X rays are produced when orbital electrons drop down to fill vacancies in the atom after an inner shell electron is displaced, usually by firing electrons at a target in a discharge tube. As the outer shell electron drops down to the vacancy it gives off energy and this is known as a characteristic X ray as the energy of the X ray is determined by the difference in the binding energies between the electron levels (Fig. 2.5).

As any orbital electron can fill the vacancy, the quanta emitted in this process can take a number of energies. The spectrum is characteristic, however, for the target metal and this forms the basis of quantitative X-ray spectroscopy for sample analysis. The spectrum of energies emerging in X-ray emission displays a continuous nature, however, and this is due to a second process for X-ray production known as Bremsstrahlung (*German*: "braking radiation").

Bremsstrahlung radiation is produced after a free electron with kinetic energy is decelerated by the influence of a heavy target nucleus. The electron and the nucleus interact via a Coulomb (electrostatic charge) interaction, the nucleus being positively charged and the electron carrying a single negative charge. The process is illustrated in Fig. 2.6. The electron loses kinetic energy after its deceleration under the influence of the target nucleus, which is given off as electromagnetic radiation. There will be a continuum of quantized energies possible in this process depending on the energy of the electron, the size of the nucleus, and other physical factors, and this gives the continuous component of the X-ray spectrum. The efficiency of Bremsstrahlung radiation production is highly dependent on the atomic number of the nucleus, with the fraction of positron energy converted to electromagnetic radiation being approximately equal to ZE/3000, where Z is the atomic number of the absorber and E is the positron energy in MeV. For this reason, low Z materials such as perspex are preferred for shielding positron emitters.

X rays generally have energies in the range of ~10^3–10^5 eV.

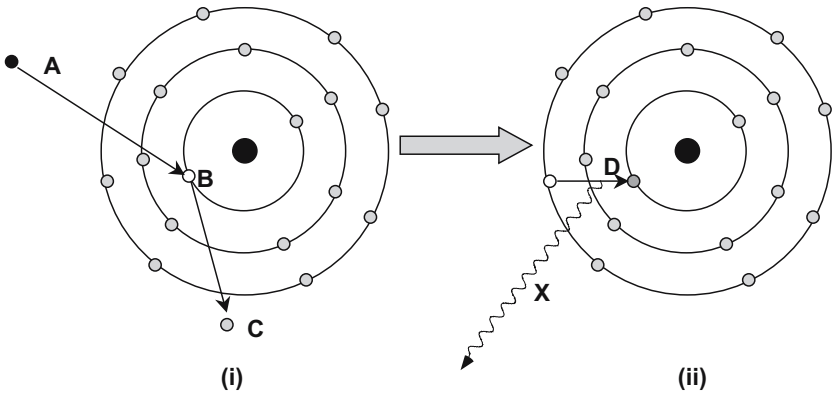

Figure 2.5. The characteristic X-ray production process is shown. In (i) an electron(A) accelerated in a vacuum tube by an electric field gradient strikes the metal target and causes ionization of the atom; in this case in the k-shell. The electron (B) is ejected from the atom (C). Subsequently (ii), a less tightly bound outer orbital electron fills the vacancy (D) and in doing so gives up some energy (X), which comes off at a characteristic energy equal to the difference in binding energy between the two energy levels. The radiation produced is an X ray.

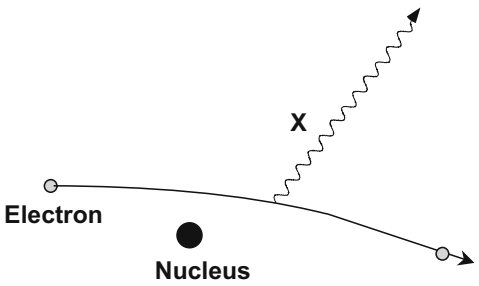

Figure 2.6. The Bremsstrahlung process is responsible for the continuous spectrum of X rays.

Gamma Radiation

Gamma rays are electromagnetic radiation emitted from the nucleus after a spontaneous nuclear decay. This is usually associated with the emission of an alpha or beta particle although there are alternative decay schemes. X and γ rays are indistinguishable after they are emitted from the atom and only differ in their site of origin. After the emission of a particle in a radioactive decay the nucleus can be left in an excited state and this excess energy is given off as a γ ray, thus conserving energy.

Gamma ray emission is characteristic, and it is determined by the difference in energy levels between the initial and final state of the energy level transitions within the nucleus.

Annihilation Radiation

As this book is primarily concerned with positrons and their applications, we include a further classification for electromagnetic radiation which is neither x nor γ. *Annihilation radiation* is the energy produced by the positron–electron annihilation process. The energy of the radiation is equivalent to the rest mass of the electron and positron, as we saw in the section on Mass and Energy, above. The mechanism of positron decay is discussed in depth in the next section.

Annihilation radiation, arising from positron–electron annihilation, is produced outside of the nucleus, and often outside of the positron-emitting atom. There are two photons produced by each positron decay and annihilation. Each photon has energy of 0.511 MeV, and the photons are given off at close to 180° opposed directions. It is this property of collinearity that we exploit in PET, allowing us to define the line-of-sight of the event without the need for physical collimation.

Particulate Radiation

Particle emission from natural radioactive decay was the first observation of radioactivity. Wilhelm Röntgen had produced X rays in 1896, and a year later Henri Becquerel showed that naturally occurring uranium produced radiation spontaneously. While the radiation was thought initially to be similar to Röntgen's x rays, Rutherford showed that some types of radiation were more penetrating than others. He called the less penetrating radiation alpha (α) rays and the more penetrating ones beta (β) rays. Soon after, it was shown that these radiations could be deflected by a magnetic field, i.e., they carried charge. It was clear that these were not electromagnetic rays and were, in fact, particles.

Radioactive Decay

The rate at which nuclei spontaneously undergo radioactive decay is characterized by the parameter called the half-life of the radionuclide. The half-life is the time it takes for half of the unstable nuclei present to decay (Fig. 2.7). It takes the form of an exponential function where the number of atoms decaying at any particular instant in time is determined by the number of unstable nuclei present and the decay constant (λ) of the nuclide. The rate of decay of unstable nuclei at any instant in time is called the *activity* of the radionuclide. The activity of the nuclide after a time t is given by

$$A_t = A_0 e^{-\lambda t} \tag{5}$$

where A_0 is the amount of activity present initially, A_t is the amount present after a time interval t, and λ is the decay constant. The decay constant is found from

$$\lambda = \frac{\log_e (2)}{t_{\frac{1}{2}}} \tag{6}$$

and the units for λ are time^{-1}. The SI unit for radioactivity is the becquerel (Bq). One becquerel (1 Bq) equals one disintegration per second.

Example: calculate the radioactivity of a 100 MBq sample of ^{18}F ($t_{\frac{1}{2}}$ = 109.5 mins) 45 minutes after calibration and from this deduce the number of atoms and mass of the radionuclide present:

$$\lambda = \frac{0.6931}{109.5} = 6.330 \times 10^{-3} \text{ min}^{-1}$$

$$A_t = 100 \times e^{-6.330 \times 10^{-3} x\, 45} \tag{7}$$

$$= 75.2 \text{ MBq}$$

The total number of ^{18}F atoms present, N, can be calculated from the activity and the decay constant using:

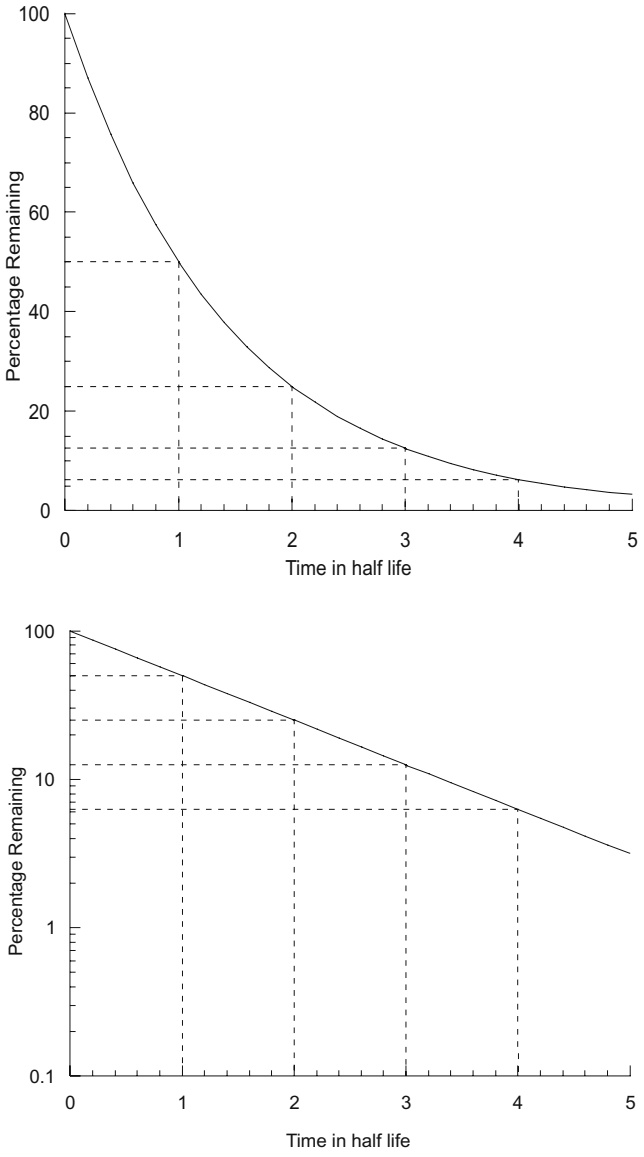

Figure 2.7. The decay of a radionuclide follows an exponential form seen in the top graph, which gives a straight line in the log-linear plot on the bottom. The dashed lines indicate the amount remaining after each half-life.

$$N = \frac{A_t}{\lambda} \tag{8}$$

In this example the total number of ^{18}F nuclei present would be:

$$N = \frac{75.2 \times 10^6}{1.055 \times 10^{-4}\ (\text{sec}^{-1})} \tag{9}$$
$$= 7.13 \times 10^{11} \text{ nuclei}$$

We can determine the mass of this number of nuclei using Avogadro's number ($N_A = 6.023 \times 10^{23}$ mole^{-1}) and the mass of a mole of ^{18}F (18 g) to be

$$m = \frac{N}{N_A} = \frac{7.13 \times 10^{11}}{6.023 \times 10^{23}} \times 18 \text{ g}$$
$$= 2.13 \times 10^{-11} g \text{ (21.3 pg)} \tag{10}$$

There are two other terms related to radioactivity that are useful. *Specific Activity* is the ratio of radioactivity to total mass of the species present. It has units of TBq/gm or TBq/mole. *Branching ratio* is the fraction of atoms that decay by the emission of a particular radiation. For example, ^{11}C is a pure positron emitter and therefore has a branching ratio of 1.00 (or 100%). ^{18}F, however, decays to ^{18}O by positron emission only 96.9% of the time, the remaining time being by electron capture (EC) which does not emit a positron. Its branching ratio is 0.969 (or 96.9%). Note that the radioactivity of a nuclide is the number of atoms decaying per second, not the number of radiation particles given off. Thus, to calculate the radioactivity from a measurement of the emitted rate of particles or photons, a correction is required to account for the non-radiative disintegrations.

Correcting for decay is often required in calculations involving radioactivity. The decay correction factor can be calculated from the point in time of an instantaneous measurement to a reference time. The decay correction factor (F) is given by:

$$F = e^{\lambda(t-t_0)} \tag{11}$$

where t is the time of the measurement and t_0 is the reference time. It is often necessary to account for decay *within* the interval of the counting period, especially with short-lived tracers as are used in positron imaging. The correction factor (F_{int}) to account for decay during a measurement is:

$$F_{\text{int}} = \frac{\lambda t}{1 - e^{-\lambda t}} \tag{12}$$

although taking the time t from the *mid-point* of the counting interval (rather than the time at the start of the measurement) to the reference time in the calculation of F introduces an error of typically less than 1% for counting intervals $<0.75 t_{\frac{1}{2}}$.

Alpha Decay

Alpha particles are helium nuclei ($^4_2He^{2+}$). They are typically emitted from high Z-number atoms and form the components of many naturally occurring radioactive decay series. Due to their large mass, alpha particles deposit large amounts of energy in a very small distance in matter. Therefore, as a radiation hazard they represent a very large problem if ingested, however, conversely, as they are relatively easy to stop,

they are easily shielded. An example of alpha decay is shown in the following:

$$^{238}_{92}\mathrm{U} \rightarrow ^{234}_{90}\mathrm{Th} + ^{4}_{2}\alpha + \gamma \quad (13)$$

The half-life for this particular process is 4.5×10^9 years.

Beta Decay

Beta particles are negatively charged electrons that are emitted from the nucleus as part of a radioactive disintegration. The beta particles emitted have a continuous range of energies up to a maximum. This appeared at first to be a violation of the conservation of energy. To overcome this problem, in 1931 Wolfgang Pauli proposed that another particle was emitted which he called the neutrino (ν). He suggested that this particle had a very small mass and zero charge. It could carry away the excess momentum to account for the difference between the maximum beta energy and the spectrum of energies that the emitted beta particles displayed. In fact, we now refer to the neutrino emitted in beta-minus decay as the *antineutrino*, indicated by the '–' over the symbol ν. β^- decay is an example of a weak interaction, and is different to most other fundamental decays as parity is not conserved.

The following shows an example of a beta decay scheme for ^{131}I:

$$^{131}_{53}I \rightarrow ^{131}_{54}Xe + ^{0}_{-1}\beta^- + \gamma + \bar{\nu} \quad (14)$$

The half-life for ^{131}I decay is 8.02 days. The most abundant β particle emitted from ^{131}I has a maximum energy of 0.606 MeV and there are many associated γ rays, the most abundant (branching ratio = 0.81) having an energy of 0.364 MeV.

Positron Decay

There are two methods of production of positrons: by pair production, and by nuclear transmutation. Pair production will be discussed in the following section. Positron emission from the nucleus is secondary to the conversion of a proton into a neutron as in:

$$^{1}_{1}p^+ \rightarrow ^{1}_{0}n + ^{0}_{1}\beta^+ + \nu \quad (15)$$

with in this case a neutrino is emitted. The positron is the antimatter conjugate of the electron emitted in β^- decay.

The general equation for positron decay from an atom is:

$$^{A}_{Z}X \rightarrow ^{A}_{Z-1}Y + ^{0}_{1}\beta^+ + \nu + Q\,(+e^-) \quad (16)$$

where Q is energy. The atom X is proton-rich and achieves stability by converting a proton to a neutron. The positive charge is carried away with the positron. As the daughter nucleus has an atomic number one less than the parent, one of the orbital electrons must be ejected from the atom to balance charge. This is often achieved by a process known as *internal conversion*, where the nucleus supplies energy to an orbital electron to overcome the binding energy and leave it with residual kinetic energy to leave the atom. As both a positron and an electron are emitted in positron decay the daughter nucleus must be at least two electron masses lighter than the parent.

The positron will have an initial energy after emission, which, similar to the case of β^- decay, can take a continuum of values up to a maximum. After emission from the nucleus, the positron loses kinetic energy by interactions with the surrounding matter. The positron interacts with other nuclei as it is deflected from its original path by one of four types of interaction:

(i) *Inelastic collisions* with atomic electrons, which is the predominant mechanism of loss of kinetic energy,
(ii) *Elastic scattering* with atomic electrons, where the positron is deflected but energy and momentum are conserved,
(iii) *Inelastic scattering* with a nucleus, with deflection of the positron and often with the corresponding emission of Bremsstrahlung radiation,
(iv) *Elastic scattering* with a nucleus where the positron is deflected but does not radiate any energy or transfer any energy to the nucleus.

As the positron passes through matter it loses energy constantly in ionisation events with other atoms or by radiation after an inelastic scattering. Both of these situations will induce a deflection in the positron path, and thus the positron takes an extremely tortuous passage through matter. Due to this, it is difficult to estimate the range of positrons based on their energy alone, and empirical measurements are usually made to determine the mean positron range in a specific material.

The positron eventually combines with an electron when both are essentially at rest. A metastable intermediate species called positronium may be formed by the positron and electron combining. Positronium is a non-nuclear, hydrogen-like element composed of the positron and electron that revolve around their combined centre of mass. It has a mean life of around 10^{-7} seconds. As expected, positronium displays similar properties to the hydrogen atom with its spectral lines having approximately half the frequency of those of hydrogen due to the much smaller mass ratio. Positronium formation occurs with a high probability

Table 2.3. Properties of some positron-emitting nuclides of interest in PET compiled from a variety of sources.

Nuclide	E_{max} (MeV)	E_{mode} (MeV)	$t_{\frac{1}{2}}$ (mins)	Range in Water (mm) Max	Mean	Use in PET
^{11}C	0.959	0.326	20.4	4.1	1.1	Labelling of organic molecules
^{13}N	1.197	0.432	9.96	5.1	1.5	$^{13}NH_3$
^{15}O	1.738	0.696	2.03	7.3	2.5	$^{15}O_2$, $H_2{}^{15}O$, $C^{15}O$, $C^{15}O_2$
^{18}F	0.633	0.202	109.8	2.4	0.6	[^{18}F]-DG, $^{18}F^-$
^{68}Ga	1.898	0.783	68.3	8.2	2.9	[^{68}Ga]-EDTA, [^{68}Ga]-PTSM
^{82}Rb	3.40	1.385	1.25	14.1	5.9	Generator-produced perfusion tracer
^{94m}Tc	2.44	†	52	‡	‡	β^+-emitting version of ^{99m}Tc
^{124}I	2.13	†	6.0×10^3	‡	‡	Iodinated molecules

‡Not reported to date.
†Many-positron decay scheme hence no E_{mode} value given.

in gases and metals, but only in about one-third of cases in water or human tissue where direct annihilation of the electron and the positron is more favorable. Positronium can exist in either of two states, para-positronium (spin = $+\frac{1}{2}$) or orthopositronium (spin = $+\frac{3}{2}$). Approximately three-quarters of the positronium formed is orthopositronium.

Positron emission from the nucleus, with subsequent annihilation, means that the photon-producing event (the annihilation) occurs outside the radioactive nucleus. The finite distance that positrons travel after emission contributes uncertainty to the localisation of the decaying nucleus (the nucleus is the species that we wish to determine the location of in positron tomography, not where the positron eventually annihilates). The uncertainty due to positron range is a function that increases with increasing initial energy of the positron. For a high-energy positron such as ^{82}Rb (E_{max} = 3.4 MeV), the mean range in water is around 5.9 mm. Table 3.3 shows some commonly used positron emitting nuclides and associated properties.

When the positron and electron eventually combine and annihilate electromagnetic radiation is given off. The most probable form that this radiation takes is of two photons of 0.511 MeV (the rest-mass equivalent of each particle) emitted at 180° to each other, however, three photons can be emitted (<1% probability). The photons are emitted in opposed directions to conserve momentum, which is close to zero before the annihilation.

Many photon pairs are not emitted strictly at 180°, however, due to non-zero momentum when the positron and electron annihilate. This fraction has been estimated to be as high as 65% in water. This con-

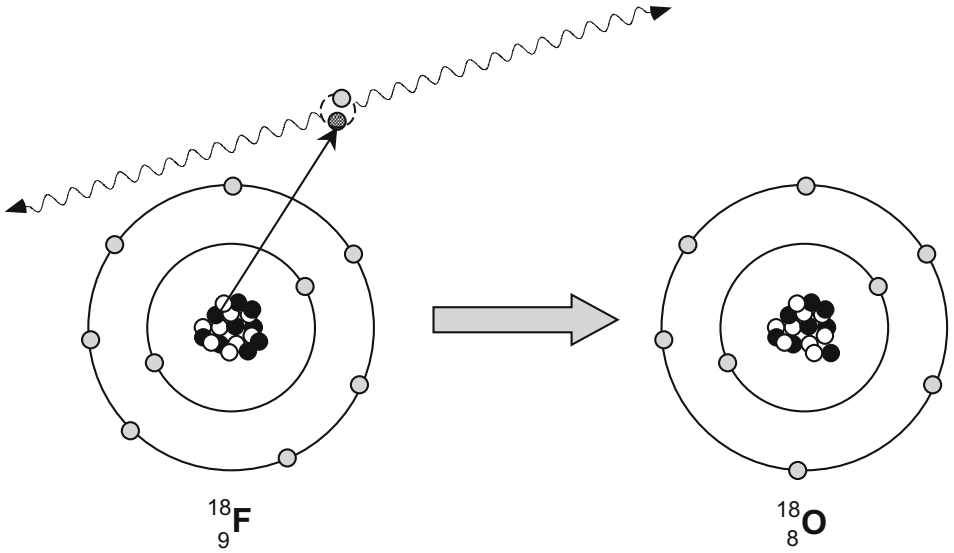

Figure 2.8. Annihilation radiation is produced subsequent to a positron being ejected from the nucleus. The positron travels a finite distance, losing energy by interaction with other electrons and nuclei as it does, until it comes to rest and combines (annihilates) with an electron to give rise to two photons, each equivalent to the rest-mass energy of the particles. The two photons are approximately anti-collinear and it is this property that is used to localize events in PET.

tributes a further uncertainty to the localisation of the nuclear decay event of 0.5° FWHM from strictly 180°, which can degrade resolution by a further 1.5 mm (dependent on the distance between the two coincidence detectors). This effect, and the finite distance travelled by the positron before annihilation, places a fundamental lower limit of the spatial resolution that can be achieved in positron emission tomography.

Interaction of Radiation with Matter

When high-energy radiation interacts with matter energy can be transferred to the material. A number of effects may follow, but a common outcome is the ionisation or excitation of the atoms in the absorbing material.

In general, the larger the mass of the particle the greater the chance of being absorbed by the material. Large particles such as alpha particles have a relatively short range in matter, whereas beta particles are more penetrating. The extremely small mass of the neutrino, and the fact that it has no charge, means that it interacts poorly with material, and is very hard to stop or detect. High-energy photons, being massless, are highly penetrating.

Interaction of Particulate Radiation with Matter

When higher energy particles such as alphas, betas, protons, or deuterons interact with atoms in an absorbing material the predominant site of interaction is with the orbital electrons of the absorber atoms. This leads to ionisation of the atom, and liberation of excited electrons by the transfer of energy in the interaction. The liberated electrons themselves may have sufficient energy to cause further ionisation of neighboring atoms and the electrons liberated from these subsequent interactions are referred to as delta rays.

Positron annihilation is an example of a particulate radiation interacting with matter. We have already examined this process in detail.

Interaction of Photons with Matter

High-energy photons interact with matter by three main mechanisms, depending on the energy of the electromagnetic radiation. These are (i) the photoelectric effect, (ii) the Compton effect, and (iii) pair production. In addition, there are other mechanisms such as coherent (Rayleigh) scattering, an interaction between a photon and a whole atom which predominates at energies less than 50 keV; triplet production and photonuclear reactions, where high energy gamma rays induce decay in the nucleus, and which require energies of greater than ~10 MeV. We will focus on the three main mechanisms which dominate in the energies of interest in imaging in nuclear medicine.

Photoelectric Effect

The photoelectric effect occupies a special place in the development of the theory of radiation. During the course of experiments which demonstrated that light acted as a wave, Hertz and his student Hallwachs showed that the effect of an electric spark being induced in a circuit due to changes in a nearby circuit could be enhanced if light was shone upon the gap between the two coil ends. They went on to show that a negatively charged sheet of zinc could eject negative charges if light was shone upon the plate. Philipp Lenard demonstrated in 1899 that the light caused the metal to emit electrons. This phenomenon was called the photoelectric effect. These experiments showed that the electric current induced by the ejected electrons was directly proportional to the intensity of the light. The interesting aspect of this phenomenon was that there appeared to be a light intensity threshold below which no current was produced. This was difficult to explain based on a continuous wave theory of light. It was these observations that led Einstein to propose the quantized theory of the electromagnetic radiation in 1905, for which he received the Nobel Prize.

The photoelectric effect is an interaction of photons with orbital electrons in an atom. This is shown in Fig. 2.9. The photon transfers all of its energy to the electron. Some of the energy is used to overcome the

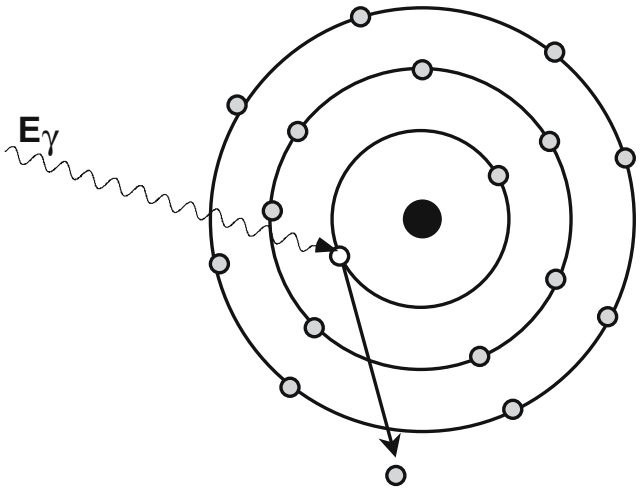

Figure 2.9. The photoelectric effect involves all of the energy from a photon being transferred to an inner shell electron, causing ionization of the atom.

binding energy of the electron, and the remaining energy is transferred to the electron in the form of kinetic energy. The photoelectric effect usually occurs with an inner shell electron. As the electron is ejected from the atom (causing ionisation of the atom) a more loosely bound outer orbital electron drops down to occupy the vacancy. In doing so it will emit radiation itself due to the differences in the binding energy for the different electron levels. This is a characteristic X ray. The ejected electron is known as a photoelectron. Alternately, instead of emitting an X ray, the atom may emit a second electron to remove the energy and this electron is known as an Auger electron. This leaves the atom doubly charged. Characteristic X rays and Auger electrons are used to identify materials using spectroscopic methods based on the properties of the emitted particles.

The photoelectric effect dominates in human tissue at energies less than approximately 100 keV. It is of particular significance for X-ray imaging, and for imaging with low-energy radionuclides. It has little impact at the energy of annihilation radiation (511 keV), but with the development of combined PET/CT systems, where the CT system is used for attenuation correction of the PET data, knowledge of the physics of interaction via the photoelectric effect is extremely important when adjusting the attenuation factors from the X-ray CT to the values appropriate for 511 keV radiation.

Compton Scattering

Compton scattering is the interaction between a photon and a loosely bound orbital electron. The electron is so loosely connected to the atom that it can be considered to be essentially free. This effect dominates in human tissue at energies above approximately 100 keV and less than ~2 MeV. The binding potential of the electron to the atom is extremely small compared with the energy of the photon, such that it can be considered to be negligible in the calculation. After the interaction, the photon undergoes a change in direction and the electron is ejected from the atom. The energy loss by the photon is divided between the small binding energy of the energy level and the kinetic energy imparted to the Compton recoil electron. The energy transferred does not depend on the properties of the material or its electron density (Fig. 2.10).

The energy of the photon after the Compton scattering can be calculated from the Compton equation:

$$E'_\gamma = \frac{E_\gamma}{1+\frac{E_\gamma}{m_0c^2}(1-\cos(\theta_c))} \tag{17}$$

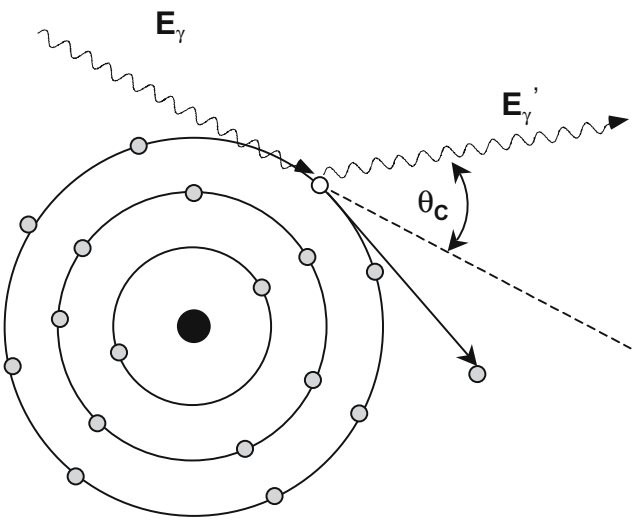

Figure 2.10. In Compton scattering, part of the energy of the incoming photon is transferred to an atomic electron. This electron is known as the recoil electron. The photon is deflected through an angle proportional to the amount of energy lost.

e.g., What is the energy of an annihilation photon after a single scatter through 60°?

$$E_\gamma = 511 \text{ keV} \tag{18}$$

$$\theta_c = 60°;\ \cos[\theta_c] = 0.5 \tag{19}$$

$$m_0c^2 = 9.11\times10^{-31} \text{ kg} \times (3.0\times10^8 \text{ m}\cdot\text{s}^{-1})^2 \equiv 511 \text{ keV} \tag{20}$$

$$E'_\gamma = \frac{511}{1+\frac{511}{511}(1-0.5)} = 341\ keV \tag{21}$$

From consideration of the Compton equation it can be seen that the maximum energy loss occurs when the scattering angle is 180° (cos (180°) = −1), i.e., the photon is *back-scattered*. A 180° back-scattered annihilation photon will have an energy of 170 keV.

Compton scattering is not equally probable at all energies or scattering angles. The probability of scattering is given by the Klein–Nishina equation [1]:

$$\frac{d\sigma}{d\Omega} = Zr_0^2\left(\frac{1}{1+\alpha(1-\cos\theta_C)}\right)^2\left(\frac{1+\cos^2\theta}{2}\right)\left(1+\frac{\alpha^2(1-\cos\theta_C)^2}{(1+\cos^2\theta_C)(1+\alpha\{1-\cos\theta_C\})}\right) \tag{22}$$

where $d\sigma/d\Omega$ is the differential scattering cross-section, Z is the atomic number of the scattering material, r_0 is the classical electron radius, and $\alpha = E_\gamma/m_0c^2$. For positron annihilation radiation (where $\alpha = 1$) in tissue,

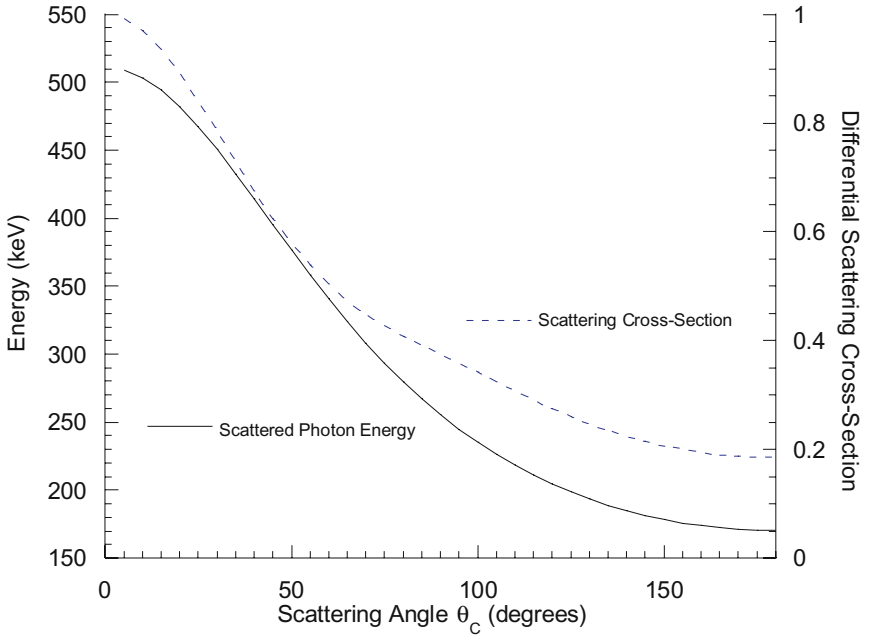

Figure 2.11. The angular probability distribution (differential scattering cross-section, broken line) and resultant energy (solid line) for Compton-scattered annihilation photons are shown.

this equation can be reduced for first-order scattered events to give the relative probability of scatter as:

$$\frac{d\sigma}{d\Omega} = \left(\frac{1}{2-\cos\theta_C}\right)^2 \left(1 + \frac{(1-\cos\theta_C)^2}{(2-\cos\theta_C)(1+\cos^2\theta_C)}\right) \quad (23)$$

Figure 2.11 shows the form that this function takes in the range 0–180°. A number of Monte Carlo computer simulation studies of the interaction of annihilation radiation with tissue-equivalent material in PET have shown that the vast majority (>80%) of scattered events that are detected have only undergone a single scattering interaction.

Pair production: The final main mechanism for photons to interact with matter is by pair production. When photons with energy greater than 1.022 MeV (twice the energy equivalent to the rest mass of an electron) pass in the vicinity of a nucleus it is possible that they will spontaneously convert to two electrons with opposed signs to conserve charge. This direct electron pair production in the Coulomb field of a nucleus is the dominant interaction mechanism at high energies (Fig. 2.12). Above the threshold of 1.022 MeV, the probability of pair production increases as energy increases. At 10 MeV, this probability is about 60%. Any energy left over after the production of the electron–positron pair is shared between the particles as kinetic energy, with the positron having slightly higher kinetic energy than the electron as the interaction of the particles with the nucleus causes an acceleration of the positron and a deceleration of the electron.

Pair production was first observed by Anderson using cloud chambers in the upper atmosphere, where high-energy cosmic radiation produced tracks of diverging ionisation left by the electron–positron pair.

The process of pair production demonstrates a number of conservation laws. *Energy* is conserved in the process as any residual energy from the photon left over after the electron pair is produced (given by $E_\gamma - 2m_0 c^2$) is carried away by the particles as kinetic energy; *charge* is conserved as the incoming photon

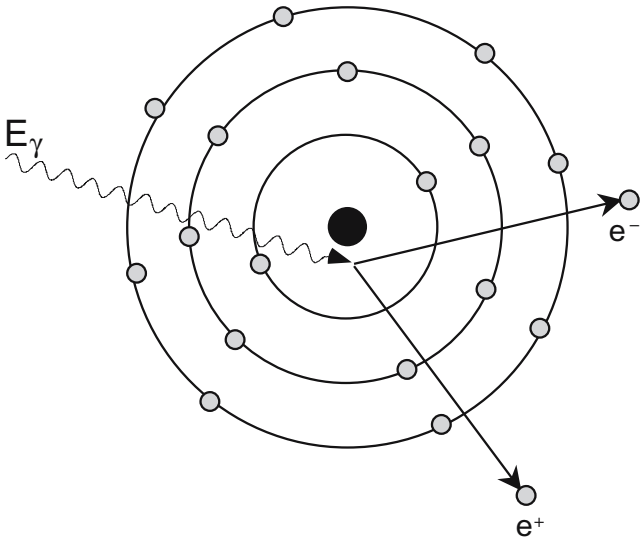

Figure 2.12. The pair production process is illustrated. As a photon passes in the vicinity of a nucleus spontaneous formation of positive and negatively charged electrons can occur. The threshold energy required for this is equal to the sum of the rest masses for the two particles (1.022 MeV).

has zero charge and the outgoing positive and negative electrons have equal and opposite charge; and *momentum* is conserved as the relatively massive nucleus absorbs momentum without appreciably changing its energy balance.

Electron–positron pair production offered the first experimental evidence of Dirac's postulated "antimatter", i.e., that for every particle in the universe there exists a "mirror image" version of it. Other particles can produce matter/antimatter pairs, such as protons, but, as the mass of the electron is much less than a proton, a photon of lower energy is required for electron–positron pair production, thus making the process more probable. The particles produced will behave like any other free electron and positron, causing ionisation of other atoms, and the positron will annihilate with an orbital electron, producing annihilation radiation as a result.

At energies above four rest-mass equivalents of the electron, pair production can take place in the vicinity of an electron. In this case it is referred to as "triplet production" as there is a third member of the interaction, the recoiling electron.

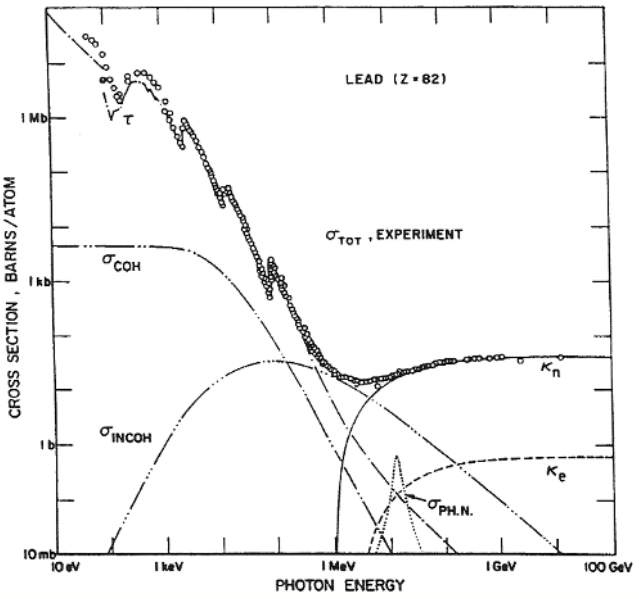

Figure 2.13. Total atomic cross-section as a function of photon energy for lead. The scattering cross-sections (σ) are given for coherent (COH), incoherent (INCOH) or Compton scattering, photonuclear absorption (PH.N.), atomic photoelectric effect (τ), nuclear field pair production (κ_n), electron field pair production (triplet) (κ_e), and the overall total cross section (TOT). (Reproduced with permission of the Institute of Physics Publishing from: Hubbell JH. Review of photon interaction cross section data in the medical and biological context. Phys Med Biol 1999;44(1):R1–22).

Attenuation and Scattering of Photons

In the previous section we have seen how radiation interacts with matter at an atomic level. In this section we will examine the bulk "macroscopic" aspects of the interaction of radiation with matter, with particular reference to positron emission and detection.

Calculations of photon interactions are given in terms of atomic cross sections (σ) with units of cm^2/atom. An alternative unit, often employed, is to quote the cross section for interaction in barns/atom (b/atom) where 1 barn = $10^{-24}cm^2$. The total atomic cross section is given by the sum of the cross sections for all of the individual processes [2], i.e.,

$$\sigma_{tot} = \sigma_{pe} + \sigma_{incoh} + \sigma_{coh} + \sigma_{pair} + \sigma_{tripl} + \sigma_{nph} \qquad (24)$$

where the cross sections are for the photoelectric effect (*pe*), incoherent Compton scattering (*incoh*), coherent (Rayleigh) scattering (*coh*), pair production (*pair*), triplet production (*tripl*), and nuclear photoabsorption (*nph*). Values for attenuation coefficient are often given as *mass attenuation coefficients* (μ/ρ) with units of $cm^2.g^{-1}$. The reason for this is that this value can be converted into a linear attenuation coefficient (μ_l) for any material simply by multiplying by the density (ρ) of the material:

$$\mu_l(cm^{-1}) = \mu/\rho\ (cm^2.g^{-1})\,\rho(g.cm^{-3}) \qquad (25)$$

The mass attenuation coefficient is related to the total cross section by

$$\mu/\rho\ (cm^2.g^{-1}) = \frac{\sigma_{tot}}{u(g)A} \qquad (26)$$

where $u(g) = 1.661 \times 10^{-24}$g is the atomic mass unit ($1/N_A$ where N_A is Avogadro's number) defined as $1/12^{th}$ of the mass of an atom of ^{12}C, and A is the relative atomic mass of the target element [2].

An example of the total cross section as a function of energy is shown in Fig. 2.13.

Photon Attenuation

We have seen that the primary mechanism for photon interaction with matter at energies around 0.5 MeV is by a Compton interaction. The result of this form of interaction is that the primary photon changes direction (i.e., is "scattered") and loses energy. In addition, the atom where the interaction occurred is ionized.

For a well-collimated source of photons and detector, attenuation takes the form of a mono-exponential function, i.e.,

$$I_x = I_0 e^{-\mu x} \qquad (27)$$

Table 2.4. Narrow-beam (scatter-free) linear attenuation coefficients for some common materials at 140 keV (the energy of ^{99m}Tc photons) and 511 keV (annihilation radiation).

Material	Density (ρ) [g.cm^{-3}]	μ (140 keV) [cm^{-1}]	μ (511 keV) [cm^{-1}]
Adipose tissue*	0.95	0.142	0.090
Water	1.0	0.150	0.095
Lung*	1.05¶	~0.04–0.06§	~0.025–0.04§
Smooth muscle	1.05	0.155	0.101
Perspex (lucite)	1.19	0.173	0.112
Cortical bone*	1.92	0.284	0.178
Pyrex glass	2.23	0.307	0.194
NaI(Tl)	3.67	2.23	0.34
Bismuth germanate (BGO)	7.13	~5.5	0.95
Lead	11.35	40.8	1.75

(Tabulated from Hubbell [3] and *ICRU Report 44 [4]).
¶This is the density of non-inflated lung.
§Measured experimentally.

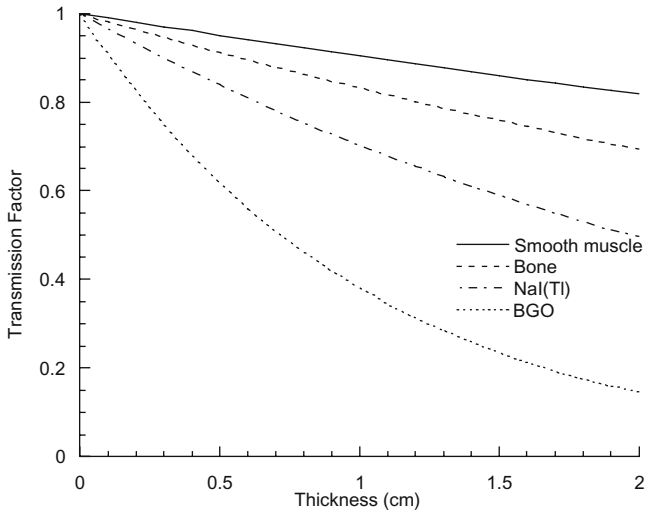

Figure 2.14. Narrow-beam transmission factors for 511 keV photons in smooth muscle, bone, NaI(Tl) and BGO as a function of the thickness of the material.

where I represents the photon beam intensity, the subscripts "0" and "x" refer respectively to the unattenuated beam intensity and the intensity measured through a thickness of material of thickness x, and m refers to the attenuation coefficient of the material (*units: cm^{-1}*). Attenuation is a function of the photon energy and the electron density (Z number) of the attenuator. The attenuation coefficient is a measure of the probability that a photon will be attenuated by a unit length of the medium. The situation of a well-collimated source and detector are referred to as *narrow-beam* conditions. The narrow-beam linear attenuation coefficients for some common materials at 140 keV and 511 keV are shown in Table 2.4 and Fig. 2.14.

However, when dealing with in vivo imaging we do not have a well-collimated source, but rather a source emitting photons in all directions. Under these uncollimated, *broad-beam* conditions, photons whose original emission direction would have taken them out of the acceptance angle of the detector may be scattered such that they are counted. The geometry of narrow and broad beam detection are illustrated in Fig. 2.15.

In the broad-beam case, an uncollimated source emitting photons in all directions contributes both unscattered and scattered events to the measurement by the detector. In this case the detector "sees" more photons than would be expected if unscattered events were excluded, and thus the transmission rate is higher than anticipated (or, conversely, attenuation appears lower). In the narrow-beam case, scattered photons are precluded from the measurement and thus the transmission measured reflects the bulk attenuating properties of the object alone.

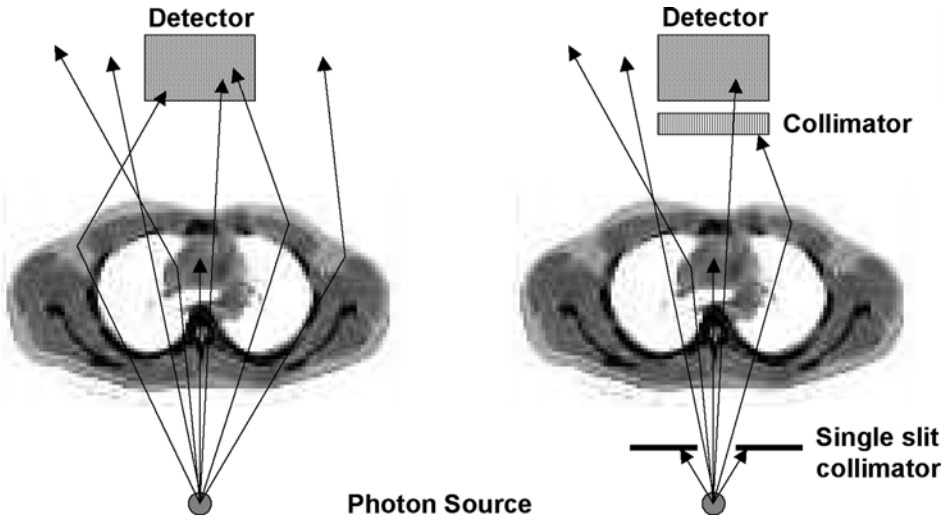

Figure 2.15. Broad-beam geometry (left) combines an uncollimated source of photons and an uncollimated detector, allowing scattered photons to be detected. The narrow-beam case (right) first constrains the photon flux to the direction towards the detector, and second, excludes scattered photons by collimation of the detector.

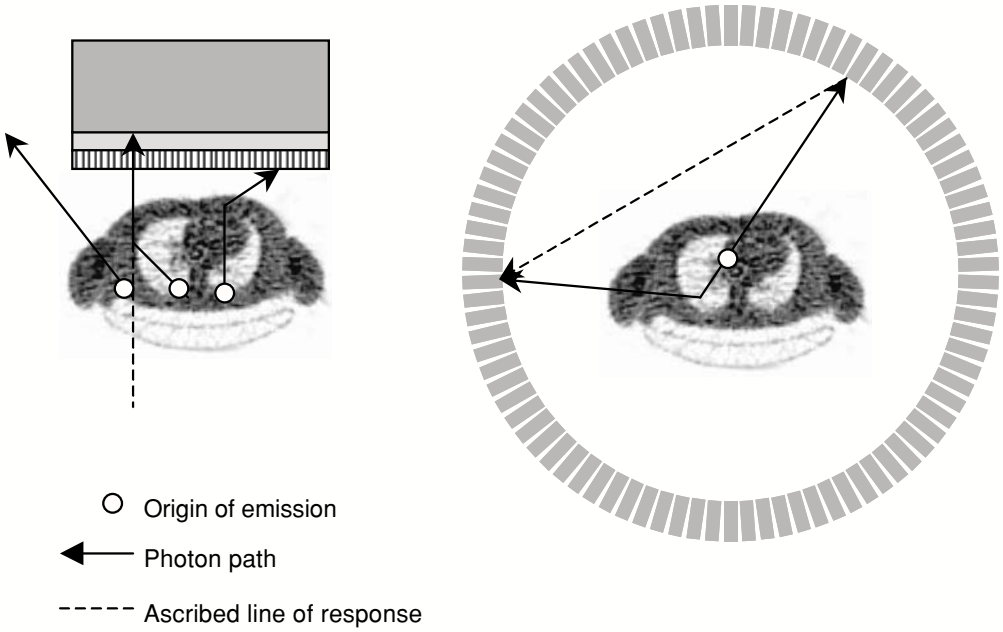

Figure 2.16. Scattered photons in SPECT and PET are shown. In SPECT, the recorded scatter is constrained within the object boundaries as there is low probability for scattering in air. In PET, as two photons are utilized, the line of response connecting the detectors may not intersect the object at all. This fact can be used to infer the underlying scatter distribution within the object by interpolation of the projections (see Ch. 6).

The geometry of scattered events is very different for PET and single photon emission computed tomography (SPECT). As PET uses coincidence detection, the line-of-sight ascribed to an event is determined by the paths taken by both annihilation photons. In this case, events can be assigned to lines of response outside of the object. This is not true in the single-photon case where, assuming negligible scattering in air, the events scattered within the object will be contained within the object boundaries. The difference in illustrated in Fig. 2.16.

Positron emission possesses an important distinction from single-photon measurements in terms of attenuation. Consider the count rate from a single photon emitting point source of radioactivity at a depth, a, in an attenuating medium of total thickness, D (see Fig. 2.17). The count rate C observed by an external detector A would be:

$$C_a = C_0 e^{-\mu a} \tag{28}$$

where C_0 represents the unattenuatted count rate from the source, and μ is the attenuation coefficient of the medium (assumed to be a constant here). Clearly the count rate changes with the depth a. If measurements were made of the source from the 180° opposed direction the count rate observed by detector B would be:

$$C_b = C_0 e^{-\mu(D-a)} \tag{29}$$

where the depth b is given by $(D - a)$. The count rate observed by the detectors will be equivalent when $a = b$.

Now consider the same case for a positron-emitting source, where detectors A and B are measuring coincident photons. The count rate is given by the *product* of the probability of counting both photons and will be:

$$\begin{aligned} C &= (C_0 e^{-\mu a}) \times (C_0 e^{-\mu(D-a)}) \\ &= C_0 \, (e^{-\mu a} \, . e^{-\mu(D-a)}) \\ &= C_0 \, e^{-\mu(a + (D-a))} \\ &= C_0 \, e^{-\mu D} \end{aligned} \tag{30}$$

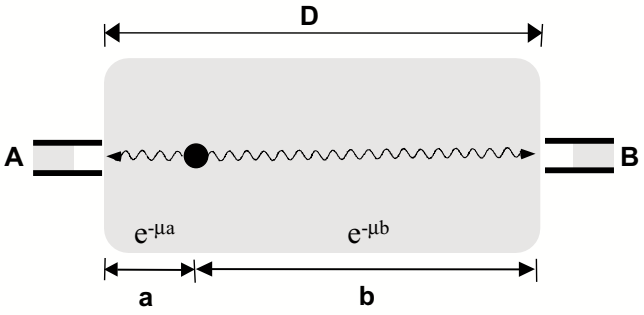

$$e^{-\mu a} \, x \, e^{-\mu b} = e^{-\mu(a+b)} = e^{-\mu D}$$

Figure 2.17. Detectors A and B record attenuated count rates arising from the source (●) located a distance a from detector A and b from detector B. For each positron annihilation, the probability of detecting both photons is the **product** of the individual photon detection probabilities. Therefore, the combined count rate observed is independent of the position of the source emitter along the line of response. The total attenuation id determined by the total thickness (D) alone.

which shows that the count rate observed in an object only depends on the total thickness of the object, D; i.e., the count rate observed is *independent* of the position of the source in the object. Therefore, to correct for attenuation of coincidence detection from annihilation radiation one measurement, the total attenuation path length ($-\mu D$), is all that is required. In single-photon measurements the depth of the source in the object, in principle, must be known as well.

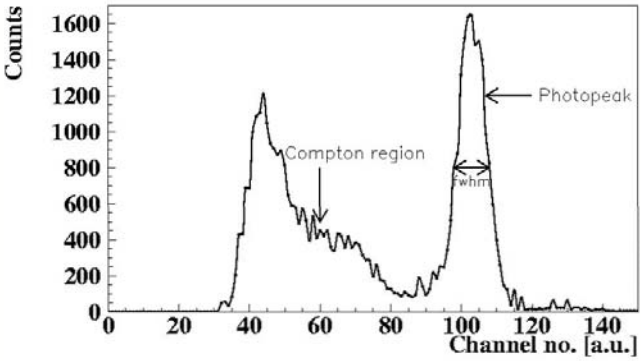

Figure 2.18. Photon energy spectrum measured by a scintillation detector.

Radiation Detection

The interactions of ionising radiation with matter form the basis upon which radiation detectors are developed. The inherent idea in these detectors is to measure the total energy lost or deposited by radiation upon passage through the detector. Typically, radiation detectors convert the deposited energy into a measurable electrical signal or charge. The integral of this signal is then proportional to the total energy deposited in the detector by the radiation. For mono-energetic incident radiation, there will be fluctuations as well as large variations in the total charge collected by the detector (see energy spectrum in Fig. 2.18). The large variations represent incomplete deposition of energy by the incident radiation. For example, in PET some of the incident 511 keV photons may undergo one or more Compton scatter, deposit a portion of their energy and then exit the detector. Multiple Compton scatter could eventually lead to deposition of almost the entire energy by the photon, thereby pushing the event into the photopeak of the energy spectrum. The continuous portion of the energy spectrum (Fig. 2.18) shows the Compton region for this measured energy spectrum with partial deposition of energy. The small fluctuations in the energy spectrum, however, arise due to several processes. The most dominant are the statistical fluctuations in the conversion process of the deposited energy into measurable charge or signal. In Fig. 2.18, the peak position marks the mean energy of the incident radiation (after complete deposition in the detector). The width of this peak (called the photopeak) shows the effect of fluctuations in the measured charge for complete deposition of energy by the mono-energetic photons. The ability of the radiation detector to accurately measure the deposited energy is of paramount importance for most of its uses. This accuracy is characterized by the width of the photopeak in the energy spectrum, and is referred to as the *energy resolution* of the detector. The energy resolution is a dimensionless number and is defined as the ratio of the full width at half maximum (FWHM) of the photopeak to its centroid position.

Radiation Detectors

Radiation detectors can generally be divided into three broad categories: proportional (gas) chambers, semiconductor detectors, and scintillation detectors.

The proportional chamber works on the principle of detecting the ionisation produced by radiation as it passes through a gas chamber. A high electric field is applied within this chamber that results in an acceleration of the ionisation electrons produced by the radiation. Subsequently, these highly energetic electrons collide with the neutral gas atoms resulting in secondary ionisations. Hence, a cascade of electrons is eventually collected at the cathode after some energy deposition by the incident radiation. Typically, inert gases such as xenon are used for detecting photons. The cathode normally consists of a single thin wire, but a fine grid of wires can be utilized to measure energy deposition as a function of position within the detector. Such position-sensitive Multi-wire Proportional Chambers (MWPC) have been used in high-energy physics for a long time, and PET scanners have been developed based upon such a detector [5, 6]. However, the disadvantage of these detectors for use in PET is the low density of the gas, leading to a reduced stopping efficiency for 511 keV photons, as well as poor energy resolution.

Another class of radiation detectors is the semiconductor or solid-state detectors. In these detectors, incident radiation causes excitation of tightly bound (valence band) electrons such that they are free to migrate within the crystal (conduction band). An applied electric field will then result in a flow of charge

through the detector after the initial energy deposition by the photons. Semiconductor detectors have excellent energy resolution but because of their production process, the stopping efficiency for 511 keV photons is low.

The third category of radiation detectors, which are of most interest to us, are the scintillation detectors. These detectors consist of an inorganic crystal (scintillator) which emits visible (scintillation) light photons after the interaction of photons within the detector. A photo-detector is used to detect and measure the number of scintillation photons emitted by an interaction. The number of scintillation photons (or intensity of light) is generally proportional to the energy deposited within the crystal. Due to their high atomic numbers and therefore density, scintillation detectors provide the highest stopping efficiency for 511 keV photons. The energy resolution, though much better than the proportional chambers, is not as good as that attained with the semiconductor detectors. This is due to the inefficient process of converting deposited energy into scintillation photons, as well as the subsequent detection by the photo-detectors. However, for PET, where both high stopping efficiency as well as good energy resolution are desired, scintillation detectors are most commonly used. For a more thorough treatment of radiation detection and measurement the reader is referred to Knoll (1988) [7].

Scintillation Detectors in PET

As mentioned above, scintillation detectors are the most common and successful mode for detection of 511 keV photons in PET imaging due to their good stopping efficiency and energy resolution. These detectors consist of an appropriate choice of crystal (scintillator) coupled to a photo-detector for detection of the visible light. This process is outlined in further detail in the next two sections.

Scintillation Process and Crystals Used in PET

The electronic energy states of an isolated atom consist of discrete levels as given by the Schrödinger equation. In a crystal lattice, the outer levels are perturbed by mutual interactions between the atoms or ions, and so the levels become broadened into a series of *allowed bands*. The bands within this series are separated from each other by the *forbidden bands*. Electrons are not allowed to fill any of these forbidden bands. The last filled band is labelled the *valence band*, while the first unfilled band is called the *conduction band*. The energy gap, E_g, between these two bands is a few electron volts in magnitude (Fig. 2.19).

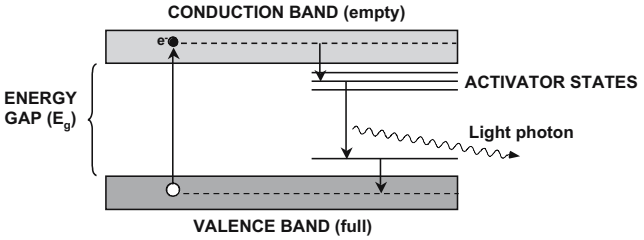

Figure 2.19. Schematic diagram of the energy levels in a scintillation crystal and the mechanism of light production after energy is absorbed. The photon energy is sufficient to move a valence band electron to the conduction band. In returning to the ground state, light photons are emitted.

Electrons in the valence band can absorb energy by the interaction of the photoelectron or the Compton scatter electron with an atom, and get excited into the conduction band. Since this is not the ground state, the electron de-excites by releasing scintillation photons and returns to its ground state. Normally, the value of E_g is such that the scintillation is in the ultraviolet range. By adding impurities to a pure crystal, such as adding thallium to pure NaI (at a concentration of ~1%), the band structure can be modified to produce energy levels in the prior forbidden region. Adding an impurity or an activator raises the ground state of the electrons present at the impurity sites to slightly above the valence band, and also produces excited states that are slightly lower than the conduction band. Keeping the amount of activator low also minimizes the self-absorption of the scintillation photons. The scintillation process now results in the emission of visible light that can be detected by an appropriate photo-detector at room temperature. Such a scintillation process is often referred to as *luminescence*. The scintillation photons produced by *luminescence* are emitted isotropically from the point of interaction. For thallium-activated sodium iodide (NaI(Tl)), the wavelength of the maximum scintillation emission is 415 nm, and the photon emission rate has an exponential distribution with a decay time of 230 ns. Sometimes the excited electron may undergo a radiation-less transition to the ground state. No scintillation photons are emitted here and the process is called *quenching*.

There are four main properties of a scintillator which are crucial for its application in a PET detector. They are: the stopping power for 511 keV photons, signal decay time, light output, and the intrinsic energy resolution. The stopping power of a scintillator is characterized by the mean distance (attenuation length = $1/\mu$) travelled by the photon before it deposits its energy within the crystal. For a PET scanner with high sensitivity, it is desirable to maximize the number of photons which interact and deposit energy in the de-

Table 2.5. Physical properties of commonly used scintillators in PET. The energy resolution and attenuation coefficients (linear (μ) and mass (μ/ρ)) are measured at 511 keV

Property	NaI(Tl)	BGO	LSO	YSO	GSO	BaF_2
Density (g/cm^3)	3.67	7.13	7.4	4.53	6.71	4.89
Effective Z	50.6	74.2	65.5	34.2	58.6	52.2
Attenuation length	2.88	1.05	1.16	2.58	1.43	2.2
Decay constant (ns)	230	300	40	70	60	0.6
Light output (photons/keV)	38	6	29	46	10	2
Relative light output	100%	15%	75%	118%	25%	5%
Wavelength λ(nm)	410	480	420	420	440	220
Intrinsic ΔE/E (%)	5.8	3.1	9.1	7.5	4.6	4.3
ΔE/E (%)	6.6	10.2	10	12.5	8.5	11.4
Index of refraction	1.85	2.15	1.82	1.8	1.91	1.56
Hygroscopic?	Yes	No	No	No	No	No
Rugged?	No	Yes	Yes	Yes	No	Yes
μ (cm^{-1})	0.3411	0.9496	0.8658	0.3875	0.6978	0.4545
μ/ρ(cm^2/gm)	0.0948	0.1332	0.117	0853	0.104	0.0929

tector. Thus, a scintillator with a short attenuation length will provide maximum efficiency in stopping the 511 keV photons. The attenuation length of a scintillator depends upon its density (ρ) and the effective atomic number (Z_{eff}). The decay constant affects the timing characteristics of the scanner. A short decay time is desirable to process each pulse individually at high counting rates, as well as to reduce the number of random coincidence events occurring within the scanner geometry (see Ch. 6). A high light-output scintillator affects a PET detector design in two ways: it helps achieve good spatial resolution with a high encoding ratio (ratio of number of resolution elements, or crystals, to number of photo-detectors) and attain good energy resolution. Good energy resolution is needed to efficiently reject events which may Compton scatter in the patient before entering the detector. The energy resolution (ΔE/E) achieved by a PET detector is dependent not only upon the scintillator light output but also the intrinsic energy resolution of the scintillator. The intrinsic energy resolution of a scintillator arises due to inhomegeneities in the crystal growth process as well as non-uniform light output for interactions within it. Table 2.5 shows the properties of scintillators that have application in PET. They are:

(i) sodium iodide doped with thallium (NaI(Tl)),
(ii) bismuth germanate $Bi_4Ge_3O_{12}$ (BGO),
(iii) lutetium oxyorthosilicate doped with cerium Lu_2SiO_5:Ce (LSO),
(iv) yttrium oxyorthosilicate doped with cerium Y_2SiO_5:Ce (YSO),
(v) gadolinium oxyorthosilicate doped with cerium Gd_2SiO_5:Ce (GSO), and
(vi) barium fluoride (BaF_2).

The energy resolution values given in this table are for single crystals. In a full PET system, variations between crystals and other factors such as light readout due to block geometry contribute to a significant worsening of the energy resolution. Typically, NaI(Tl) detectors in a PET scanner achieve a 10% energy resolution for 511 keV photons, while the BGO scanners have system energy resolution of more than 20%.

NaI(Tl) provides very high light output leading to good energy and spatial resolution with a high encoding ratio. The slow decay time leads to increased detector dead time and high random coincidences (see Energy Resolution and Scatter, below). It suffers from lower stopping power than BGO, GSO or LSO due to its lower density. BGO, on the other hand, has slightly worse timing properties than NaI(Tl) in addition to lower light output. However, the excellent stopping power of BGO gives it high sensitivity for photon detection in PET scanners. Currently, commercially produced whole-body scanners have developed along the lines of advantages and disadvantages of these two individual scintillators. The majority of scanners employ BGO and, when operating in 2D mode, use tungsten septa to limit the amount of scatter by physically restricting the axial field-of-view imaged by a detector area. This results in a reduction of the scanner sensitivity due to absorption of some photons in the septa. The low light output of BGO also requires the use of small photo-multiplier tubes to achieve good spatial resolution, thereby increasing system complexity and cost. The NaI(Tl)-based scanners [8] compromise on high count-rate performance by imaging in 3D mode in order to achieve acceptable scanner sensitivity.

LSO, a relatively new crystal, appears to have an ideal combination of the advantages of the high light output

of NaI(Tl) and the high stopping power of BGO in one crystal [9]. In spite of its high light output (~75% of NaI(Tl)), the overall energy resolution of LSO is not as good as NaI(Tl). This is due to intrinsic properties of the crystal. Another disadvantage for general applications of this scintillator is that one of the naturally occurring isotopes present (^{176}Lu, 2.6% abundance), is itself radioactive. It has a half-life of 3.8×10^{10} years and decays by β^- emission and the subsequent release of γ photons with energies from 88–400 keV. The intrinsic radioactivity concentration of LSO is approximately ~280 Bq/cc; approximately 12 counts per sec per gram would be emitted that would be detected within a 126–154 keV energy window. Thus its use in low-energy applications is restricted. This background has less impact in PET measurements due to the higher energy windows set for the annihilation radiation and the use of coincidence counting.

GSO is another scintillator with useful physical properties for PET detectors. One advantage of GSO over LSO, in spite of a lower stopping power and light output, is its better energy resolution and more uniform light output. Commercial systems are now being developed with GSO detectors.

Finally, the extremely short decay time of BaF_2 (600 psec) makes it ideal for use in time-of-flight scanners (see Time-of-flight Measurement, below), which helps to partially compensate for the low sensitivity arising due to the reduced stopping power of this scintillator.

In addition to these scintillators, which have all been used in PET tomographs already, new inorganic scintillators continue to be developed. Many of the newer scintillators are based on cerium doping of lanthanide and transition metal elements. Examples include LuAP:Ce, Y_2SiO_5 (YSO), $LuBO_3$:Ce, and others based on lead (Pb), tungsten (W) and gadolinium (Gd).

Photo-detectors and Detector Designs Used in PET

Generally, the photo-detectors used in scintillation detectors for PET can be divided into two categories, the photo-multiplier tubes (PMTs) and the semiconductor-based photodiodes. Photo-multiplier tubes (Fig. 2.20) represent the oldest and most reliable technique to measure and detect low levels of scintillation light. They consist of a vacuum enclosure with a thin photo-cathode layer at the entrance window. An incoming scintillation photon deposits its energy at the photo-cathode and triggers the release of a photo-electron. Depending upon its energy, the photo-electron can escape the surface potential of the photo-cathode and in the presence of an applied electric field accelerate to a nearby dynode which is at a positive potential with respect to the photo-cathode. Upon impact with the dynode, the electron, with its increased energy, will result in the emission of multiple secondary electrons. The process of acceleration and emission is then repeated through several dynode structures lying at in-

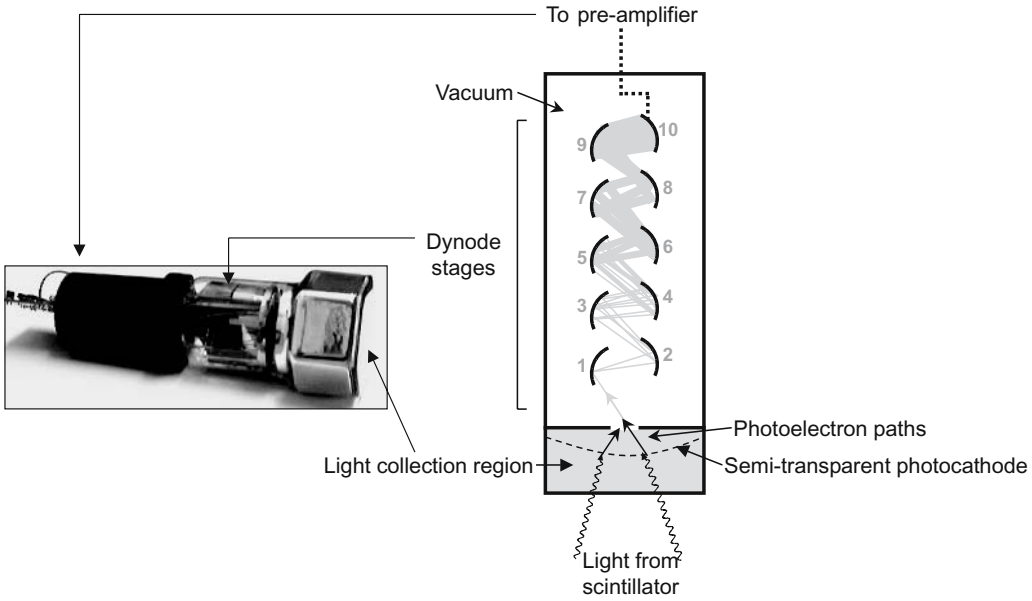

Figure 2.20. Schematic diagram of a photomultiplier tube and a photograph of a hexagonal 6 cm-diameter tube (inset). Light entering the PMT displaces a photoelectron which is electrostatically focused to the first-stage dynode. Each dynode has a positive voltage bias relative to the previous one, and so electrons are accelerated from one dynode to the next. The increase in kinetic energy acquired by this process is sufficient to displace a number of electrons at the next dynode, and so on, causing large amplification by the end-stage dynode (usually tenth or twelfth).

creasing potentials, leading to a gain of more than a million at the final dynode (anode). This high gain obtained from a photo-multiplier tube leads to a very good signal-to-noise ratio (SNR) for low light levels and is the primary reason for the success and applicability of photo-multiplier tubes for use in scintillation detectors. The only drawback of a photo-multiplier tube is the low efficiency in the emission and escape of a photo-electron from the cathode after the deposition of energy by a single scintillation photon. This property is called the *Quantum Efficiency* (QE) of the photo-multiplier tube and it is typically 25% for most of the photo-multiplier tubes. Different, complex arrangements of the dynode structure have been developed over the years in order to maximize the gain, reduce the travel time of the electrons from the cathode to the anode, as well as reduce the variation in the travel times of individual electrons. In particular, a fine grid dynode structure has been developed which restricts the spread of photoelectrons while in trajectory, thereby providing a position-sensitive energy measurement within a single photo-multiplier tube enclosure (Position Sensitive PMT or PS-PMT). More recently, a multi-channel capability has been developed which essentially reduces a single photo-multiplier tube enclosure into several very small channels. It uses a 2D array of glass capillary dynodes each of which is a few microns wide. Additionally, a multi-anode structure is used for electron collection, thereby providing a dramatically improved position-sensitive energy measurement with very little cross-talk between adjacent channels (Multi-Channel PMT, MC-PMT).

Photodiodes, on the other hand, are based upon semiconductors which, unlike the situation for detecting the photons, have high sensitivity for detecting the significantly lower energy scintillation photons. These detectors typically are in the form of PIN diodes (PIN refers to the three zones of the diode: P-type, Intrinsic, N-type). Manufacturing a PIN photodiode involves drifting an alkali metal such as lithium onto a p-type semiconductor such as doped silicon. Incident scintillation photons produce electron–hole pairs in the detector and an applied electric field then results in a flow of charge that can be measured through an external circuit. A significant disadvantage of the photodiodes is the low SNR achieved due to the presence of thermally activated charge flow and very low intrinsic signal amplification. In recent years, a new type of photodiode, called the Avalanche Photo Diode (APD), has been developed which provides an internal amplification of the signal, thereby improving the SNR. These gains are typically in the range of a few hundred and are still several orders of magnitude lower than the photo-multiplier tubes. More importantly, APD gains are sensitive to small temperature variations as well as changes in the applied bias voltage.

In general, there are three ways of arranging the scintillation crystals and coupling them to photo-detectors for signal readout in a PET detector. The first is the so-called one-to-one coupling, where a single crystal is glued to an individual photo-detector. A close-packed array of small discrete detectors can then be used as a large detector that is needed for PET imaging. The spatial resolution of such a detector is limited by the size of the discrete crystals making up the detector. In order to achieve spatial resolution better than 4 mm in one-to-one coupling, very small photo-detectors are needed. However, individual photo-multiplier tubes of this size are not currently manufactured. One solution is the use of photodiodes, or APDs instead of photo-multiplier tubes. The APDs are normally developed either as individual components or in an array, and so are ideal for use in such a detector design [10, 11]. However, as mentioned earlier, the APD gain is sensitive to variations in temperature and bias voltage that can lead to practical problems of stability in their implementation for a complete PET scanner. Another option is the coupling of individual channels of a PS-PMT or a MC-PMT to the small crystals [12]. Due to the large package size of these photo-multiplier tubes, however, clever techniques are needed to achieve a close-packed arrangement of the crystals in the scanner design. Despite the very good spatial resolution and minimal dead time achieved by the one-to-one coupling design, the inherent complexity (number of electronic channels) and cost of such PET detectors limits their use at present to research tomographs; in particular, small animal systems.

The next two detector schemes are attempts at reducing these disadvantages by increasing the encoding for the detector. Both the designs involve the use of larger photo-multiplier tubes without intrinsic position-sensing capabilities. The Anger detector, originally developed by Hal Anger in the 1950s, uses a large (*e.g.,* 1 cm thick $\times$ 30–50 cm in diameter) NaI(Tl) crystal glued to an array of photo-multiplier tubes via a light guide. This camera is normally used with a collimator to detect low-energy single photons in SPECT imaging. An application of the Anger technique to a PET detector, on the other hand, uses 2.5 cm-thick NaI(Tl) scintillators. An array of 6.5 cm-diameter photo-multiplier tubes can be used to achieve a spatial resolution of about 5 mm [8]. A weighted centroid positioning algorithm is used for estimation of the interaction position within the detector. This algorithm uses a weighted sum of the individual photo-multiplier tube signals

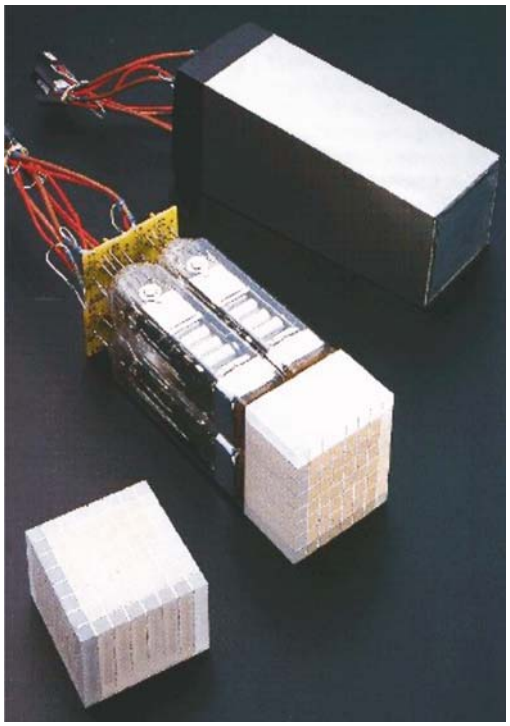

Figure 2.21. A block detector from a Siemens-CTI ECAT 951 PET scanner is shown. The sectioned (8 × 8 elements) block of BGO is in the bottom left corner, with the four square PMTs attached in the center, and the final packaged module in the top right corner. The scanner would contain 128 such modules in total, or 8192 individual detector elements. (Figure courtesy of Dr Ron Nutt, CTI PET Systems, Knoxville, TN, USA).

and normalizes it with the total signal obtained from all the photo-multiplier tubes. The weights for the photo-multiplier tube signals depend exclusively upon the photo-multiplier tube position within the array. Since these detectors involve significant light sharing between photo-multiplier tubes, a high light-output scintillator such as NaI(Tl) is needed to obtain good spatial resolution. The use of large photo-multiplier tubes produces a very high encoding ratio, leading to a simple and cost-effective design. However, a disadvantage of this detector, independent of the use of NaI(Tl) as a scintillator, is the spread of scintillation light within the crystal which leads to significant detector dead time at high count rates.

The block detector design uses Anger positioning in a restricted manner to achieve good spatial resolution and reduced dead time at the expense of a lower encoding ratio. The initial design used an 8×4 array of $6 \times 14 \times 30$ mm^3 BGO crystals glued to a slotted light guide [13]. The slots in the light guide are cut to varying depths with the deepest slots cut at the detector's edge (see Fig. 2.21, left and centre).

The read-out in this block design is performed by four 25 mm-square photo-multiplier tubes. The slotted light guide allows the scintillation light to be shared to varying degrees between the four photo-multiplier tubes depending upon the position of the crystal in which the interaction takes place. The centroid calculation is performed here as well to identify the crystal of interaction. An improved design of this detector allows the identification of smaller, $4 \times 4 \times 30$ mm^3, leading to an improved spatial resolution but with smaller 19 mm photo-multiplier tubes. Besides the advantages and disadvantages of BGO as a scintillator, the block detector design has the benefit of reduced detector dead time compared to the large-area Anger detector due to the restricted light spread. This, however, is achieved by increasing the number of detector channels (lower encoding ratio), thus leading to increased cost. A modification of the block design, called the quadrant-sharing block design [14], can distinguish smaller (half the size in either direction) crystals by straddling the 19 mm photo-multiplier tube over four block quadrants (see Fig. 2.22, right). This design, in comparison to the standard block, results in a better spatial resolution with almost double the encoding ratio, but increased detector dead time due to the use of nine photo-multiplier tubes (not four) for signal readout from an event.

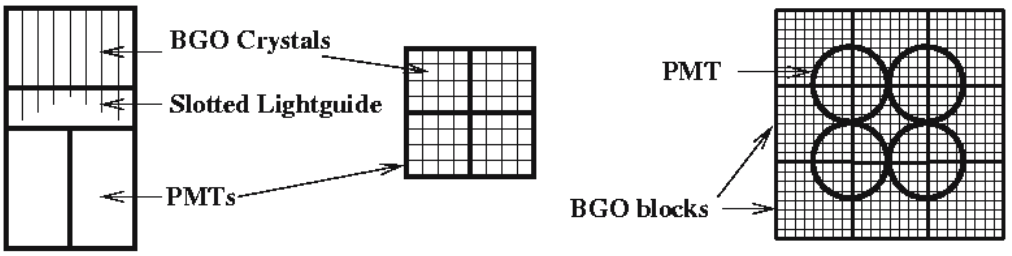

Figure 2.22. The standard block detector design from the side (left) and looking down through the crystals (middle). The quad-sharing block design as seen from the top through the crystals is shown on the right. Figures are not drawn to scale.

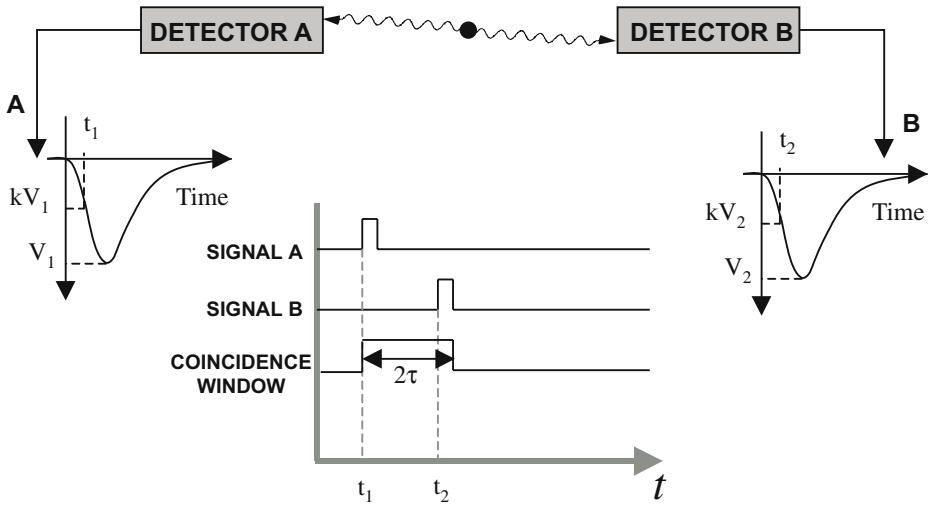

Figure 2.23. Schematic representation of detecting coincidence events in two detectors. Signal A results in a trigger pulse 1 which marks the start of the coincidence window of width Δt. Similarly, signal B results in a trigger pulse 2. A coincidence (AND) circuit then checks for coincidence between the pulse 2 and the coincidence window.

Timing Resolution and Coincidence Detection

The timing resolution of a PET detector describes the uncertainty in the timing characteristics of the scintillation detector on an event-by-event basis due to statistical fluctuations. With a fast signal (or short decay time), the timing resolution is small as well. The timing resolution of a PET detector is important because it involves the detection of two photons originating from a single coincident event. Since the timing resolution represents the variability in the signal arrival times for different events, it needs to be properly accounted for when detecting coincident events. Figure 2.23 gives a schematic representation of two detectors set up to measure coincident photons being emitted from a point equidistant from the two detectors.

The amplitude of the signal from the two detectors (V_1 and V_2 in Fig. 2.23) may be different owing to incomplete deposition of energies or varying gains of the photo-detectors in the two detectors. The coincidence circuitry, however, generates a narrow trigger pulse when the detector signals cross a certain fixed fraction of their individual amplitudes. At time t_1, signal A triggers pulse 1 which also produces a coincidence time window of a predetermined width, 2τ. Signal B, depending upon the timing resolution of the detector, will trigger at a later time, t_2. Depending upon the difference $t_2 - t_1$, the start of pulse 2 may or may not overlap with the coincidence window. For detectors with poor timing resolution, a large value for 2τ needs to be used in order to detect most of the valid coincidence events.

In a PET scanner, the two coincident photons will be emitted from anywhere within the scanner field-of-view (FOV), and so the distance travelled by each of them before interaction in the detectors will be different. For a typical whole-body scanner, this distance can be as large as the scanner diameter (about 100 cm). Using the value of speed of light ($c = 3 \times 10^8$ m/s), one can calculate an additional maximum timing difference of about 3–4 ns between the two signals (the photons travel 1 m in 3.3 ns). As a result, the coincidence timing window (2τ) of a PET detector needs to be increased even more than the requirements of the timing resolution. For an extremely fast scintillator such as BaF_2, the timing resolution is very small. However, the coincidence timing window cannot be reduced to less than 3–4 ns (in a whole-body scanner geometry) due to the difference in arrival times of two photons emitted at the edge of the scanner field of view, as this would restrict the transverse field of view.

Random Coincidences

Random coincidences are a direct consequence of having a large coincidence timing window. They arise when two unrelated photons enter the opposing detectors and are temporally close enough to be recorded within the coincidence timing window. For such events, the system produces a false coincident event. Due to the random nature of such events, they are labelled as random or accidental coincidences. Random coincidences add uncorrelated background counts to an acquired PET image and hence decrease image contrast if no corrections are applied to the acquired data. In Fig. 2.23, if signal A and signal B are unrelated, then a large coincidence timing window will result in an increased number of such events being registered as coincident events (random coincidences). The random

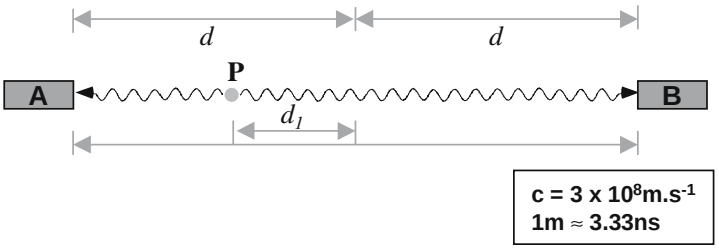

Figure 2.24. Time-of-flight measurement. P marks the annihilation point from where the two photons originate and are recorded in detectors A and B.

coincidence rate in a PET scanner is proportional to $2\tau A^2$, where A is the activity present in the scanner field of view. The true coincident rate, on the other hand, increases linearly with a given activity level in the scanner. Hence, at high activity levels, the random coincidences will overwhelm the true coincidences.

The random coincidence rate can be estimated during data collection and a correction applied to the projected data. These techniques will be outlined in further detail in the following chapters. However, it is important to point out that the random correction techniques result in a propagation of noise through the data set and so the image signal-to-noise ratio suffers. Thus, the best way to improve image contrast without reducing its signal-to-noise ratio is to minimize the collection of random coincidences. Since random coincidences are proportional to the coincidence timing window, a narrow window helps in reducing their occurrence within the detector. Hence, for PET imaging a fast scintillator with good timing resolution is desirable for reducing the number of random coincidences.

Time-of-flight Measurement

Good timing resolution of a PET detector, besides helping reduce the number of random coincidences, can also be use to estimate the annihilation point between the two detectors by looking at the difference in arrival times of the two photons. For this, an extremely fast scintillator, such as BaF_2, is needed.

In Fig. 2.24, point P marks an annihilation point which is located a distance d_1 from the point which is exactly halfway (distance d) between the two detectors. A photon moving along PA will travel a distance $d - d_1$, while the coincident photon travels a total distance $d + d_1$ along PB before entering detector B. Thus, one photon will travel an extra distance $(d + d_1) - (d - d_1) = 2d_1$ relative to the other. The coincident detectors can be used to measure the difference in arrival times (δt) of the two photons. Using the speed of light, c, for the speed of the photons, d_1 can be calculated from $2d_1 = c\delta t$. In order to obtain a good estimation of d_1, however, an accurate measurement of δt is needed, which in turn requires a fast scintillator with a timing resolution of less than 0.8 ns. Thus, the timing resolution of a PET detector introduces a blurring in the estimation of d_1. It can be shown from the above calculation that for BaF_2 with $\delta t = 0.8$ ns, a blurring of about ±6 mm is introduced in the d_1 estimation. Slow scintillators will increase this blurring significantly. Presently, only BaF_2 is feasible for use as a scintillator in time-of-flight measuring PET scanners, and such scanner designs have been successfully implemented. The advantage of estimating the location of the annihilation point is the improved signal-to-noise ratio obtained in the acquired image, arising due to a reduction in noise propagation during the image reconstruction process. However, since BaF_2 also has a very low stopping power, time-of-flight scanners have a reduced sensitivity leading to lower signal-to-noise ratios. Hence, the overall design of such scanners requires a careful trade-off between the scanner sensitivity and the time-of-flight measurement so that the overall SNR for the scanner remains high.

Energy Resolution and Scatter

The energy resolution of a radiation detector characterizes its ability to distinguish between radiation at different energies. In scintillation detectors the energy resolution is a function of the relative light output of the scintillator, as well as its intrinsic energy resolution. The intrinsic energy resolution accounts for other non-statistical effects that arise in the energy measurement process. Good energy resolution is necessary for a PET detector (especially in 3D volume imaging mode) in order to achieve good image contrast and reduce background counts in the image.

A PET scanner acquires three different kinds of coincident events: true, random, and scatter coincidences. True coincidences are emissions from single annihilation points that enter the PET detector without undergoing any significant interactions within the imaging field of view. Random coincidences, as we have already seen, arise due to the accidental detection of two unre-

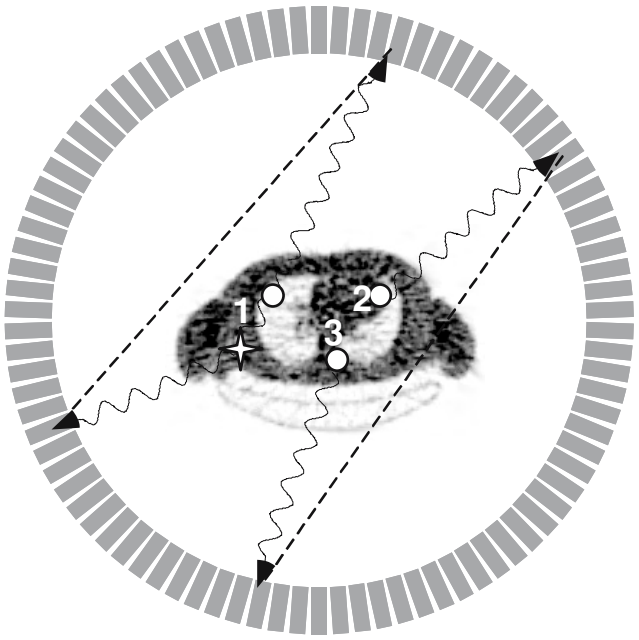

Figure 2.25. Scattered and random coincidences in a PET scanner. Event 1 shows a coincident event where one of the γ rays is scattered leading to an incorrectly assigned line-of-response (LOR, dotted) for image reconstruction (scatter coincidence). Events 2 and 3 represent two unrelated events with only one photon being detected (singles events). If they occur within the coincidence timing window, then an incorrect LOR (dotted) gets assigned (random coincidence).

lated, single events within the coincidence timing window. These coincidences add to the image background and so reduce its contrast. Finally, scatter coincidences are true coincidence events from single annihilation points, but where one or both the photons undergo Compton scatter within the imaging FOV before entering the PET detector (see Fig. 2.25). Since scattered coincidences lead to mis-positioned lines-of-response, and therefore misrepresent the true activity distribution within the FOV, the image contrast worsens.

The density of tissue in human body is approximately the same as that of water, and so the mean free path of a 511 keV photon is about 7 cm in human tissue. Since the cross-section of a human body is much greater than 7 cm, many of the photons originating inside the human body are Compton scattered before they enter the PET detectors. Since scatter involves loss of energy, in principle some of these scattered coincidences can be rejected using an energy-gating technique around the photopeak in the energy spectrum. Good energy resolution for the detector allows the application of a very narrow energy gate, and thus a more extensive and accurate rejection of scatter coincidences can be performed. However, some scattered events may be indistinguishable from true coincidences based upon the energy if they lie within the photopeak. For example, in NaI(Tl)-based detectors the good energy resolution allows the use of about 450 keV as the lower energy gate on the photopeak. Assuming only single scatter within the object, this implies that the maximum deviation from true line-of-response for scattered events within the photopeak will be about 30°. In comparison, for the BGO-based detectors, the lower energy gate is set at 300–400 keV, leading to a maximum deviation of more than 70° from the true line-of-response. Hence, additional scatter-correction techniques which estimate the distribution of scattered radiation are then employed in order to remove them from the image and improve image contrast.

Sensitivity and Depth of Interaction

The sensitivity of a PET scanner represents its ability to detect the coincident photons emitted from inside the scanner FOV. It is determined by two parameters of the scanner design; its geometry and the stopping efficiency of the detectors for 511 keV photons. Scanner geometry defines the fraction of the total solid angle covered by it over the imaging field. Small-diameter and large axial FOV typically leads to high-sensitivity scanners. The stopping efficiency of the PET detector is related to the type of detector being used. As we have seen, scintillation detectors provide the highest stopping power for PET imaging with good energy resolution. The stopping power of the scintillation detector is in turn dependent upon the density and Z_{eff} of the crystal used. Hence, a majority of commercially produced PET scanners today use BGO as the scintillator due to its high stopping power (see Table 2.4). A high-sensitivity scanner collects more coincident events in a fixed amount of time and with a fixed amount of radioactivity present in the scanner FOV. This generally translates into improved SNR for the reconstructed image due to a reduction in the effect of statistical fluctuations.

A high stopping power for the crystal is also desirable for the reduction of parallax error in the acquired images. After a photon enters a detector, it travels a short distance (determined by the mean attenuation length of the crystal) before depositing all its energy. Typically, PET detectors do not measure this point, known as the depth of interaction (DOI) within the crystal. As a result, the measured position of energy deposition is projected to the entrance surface of the detector (Fig. 2.26). For photons that enter the detector at oblique angles, this projected position can produce significant deviations from the real position, leading to a

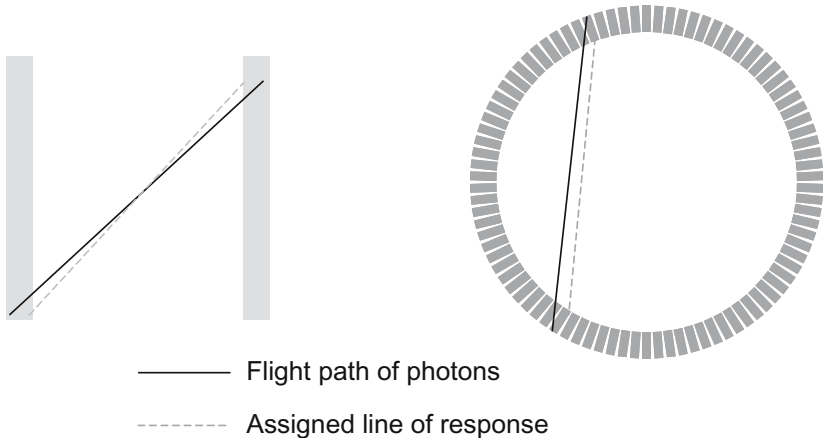

Figure 2.26. Schematic representation of parallax error introduced in the measured position due to the unknown depth-of-interaction of the photons within the detectors for a flat detector (left) and ring-based system (right).

blurring of the reconstructed image. Typically, annihilation points located at large radial distances from the scanner's central axis suffer from this parallax blurring. For a BGO whole-body scanner, measurements show that the spatial resolution worsens from 4.5 mm near the centre of the scanner to about 8.9 mm at a radial distance of 20 cm [15]. A thin crystal with high stopping power will help reduce the distance travelled by the photon in the detector and so reduce parallax effects. However, a thin crystal reduces the scanner sensitivity. Thus, to separate this inter-dependence of sensitivity and parallax error, an accurate measurement of the photon depth-of-interaction within the crystal is required.

Development of PET detectors with depth-of-interaction measurement capabilities is an ongoing research interest. Currently there are two practically feasible techniques that can be used for depth-of-interaction measurement. The first is the *phoswich* detector [16] method that involves stacking thin layers of different scintillators on top of each other, instead of using a thick layer of one crystal type. The depth-of-interaction measurement in a phoswich detector depends on the identification of interaction layer through an examination of the different signal decay times for the scintillators. As a result, the scintillators used in a phoswich detector need to have significantly different decay times in order to successfully distinguish them via pulse shape discrimination techniques. Another potential problem in its implementation is the optical coupling between the individual layers of crystals. Good optical coupling is necessary for the successful transmission of scintillation photons from the crystals into the photo-detectors, thereby achieving good spatial and energy resolution as well.

Another technique for determining the depth of interaction involves the use of photo-detectors at both the ends of a thick (or long) scintillator. This technique is based upon the physical principle according to which the relative number of scintillation photons reaching either of the end photo-detectors is a function of the photons depth of interaction in the crystal. Figure 2.27 shows a single-channel implementation of this technique. For a

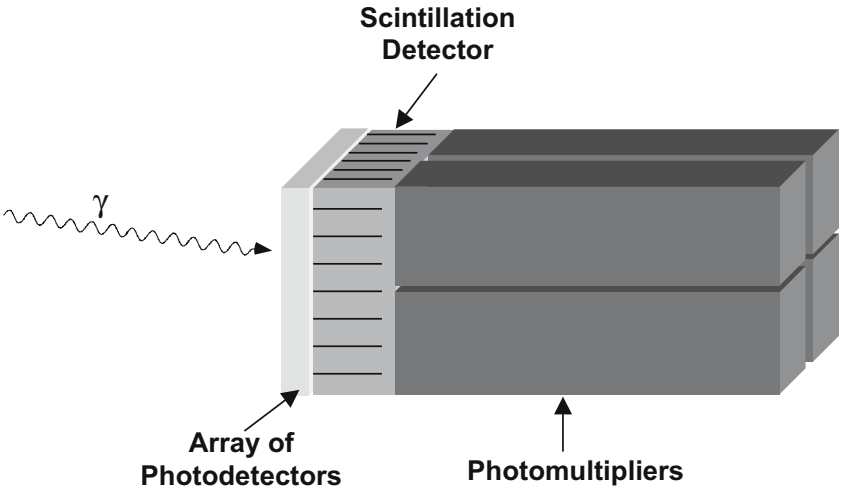

Figure 2.27. A single channel of one layer detector for DOI determination through the use of two photo-detectors at the crystal ends. In this schematic conventional light collection by PMTs are used at one end and an array of avalanche photodiodes are used on the incident face of the detector.

practical implementation in a scanner design, the use of regular photo-multiplier tubes at both ends is not feasible. As result, at least one such detector design has considered using a different type of photo-detector, such as PIN photodiodes or Avalanche photodiodes, on the crystal end that enters the scanner field of view [17].

Concluding Remarks

PET detectors and instrumentation have developed into sophisticated clinical tools, but further scope exists to develop higher-sensitivity, higher-resolution devices. There are now a number of scintillator crystals employed in commercial scanners, each with their own unique characteristics, including price. The range of scintillators may expand even further, especially if time-of-flight machines are developed. Light-collection technology may move away from photomultiplier tubes to solid-state devices (photodiodes) which will improve coupling and increase the bandwidth for data collection and processing by reducing the multiplexing of the signals.

Scanner design will continue to evolve and provide challenges in terms of photon detection, discrimination, and performance. Developments in basic physics will underpin many of these enhancements.

References

1. Klein O, Nishina Y. Uber die streuung von strahlung durch frei elektronen nach der neuen relativistischen quantendynamik von Dirac. Z Physik 1928;52:853–868.
2. Hubbell JH. Review of photon interaction cross section data in the medical and biological context. Phys Med Biol 1999;44(1):R1–22.
3. Hubbell JH. Photon cross sections, attenuation coefficients, and energy absorption coefficients from 10 keV to 100 GeV: National Bureau of Standards, US Dept of Commerce; 1969.
4. ICRU. Tissue substitutes in radiation dosimetry and measurement. Bethesda, MD, USA: International Commission on Radiation Units and Measurements; 1989. Report No. 44.
5. Townsend DW, Frey P, Jeavons A, Reich G, Tochon-Danguy HJ, Donath A, et al. High-density avalanche chamber (HIDAC) positron camera. J Nucl Med 1987;28:1554–62.
6. Jeavons AP, Chandler RA, Dettmar CAR. A 3D HIDAC-PET camera with sub-millimetre resolution for imaging small animals. IEEE Trans Nucl Sci 1999;NS-46:468–73.
7. Knoll GF. Radiation detection and measurement. 2nd ed. New York: John Wiley and Sons; 1988.
8. Karp JS, Muehllehner G, Geagan MJ, Freifelder R. Whole-body PET scanner using curve-plate NaI(Tl) detectors. J Nucl Med 1998;39:50P(abstract).
9. Melcher CL, Schweitzer JS. Cerium-doped lutetium oxyorthorthsilicate: a fast, efficient new scintillator. IEEE Trans Nucl Sci 1992;39(4):502–5.
10. Lecomte R, Cadorette J, Richard P et al. Design and engineering aspects of a high-resolution positron tomograph for small-animal imaging. IEEE Trans Nucl Sci 1996;NS-41(4):1446–52.
11. Ziegler SI, Pichler BJ, Boening G, Rafecas M, Pimpl W, Lorenz E, et al. A prototype high-resolution animal positron tomograph with avalanche photodiode arrays and LSO crystals. Eur J Nucl Med 2001;28:136–43.
12. Cherry SR, Shao Y, Silverman RW, Chatziioannou A, Meadors K, Siegel S, et al. MicroPET: A high-resolution PET scanner for Imaging small animals. IEEE Trans Nucl Sci 1997;44:1161–6.
13. Casey ME, Nutt R. A multicrystal, two-dimensional BGO detector system for positron emission tomography. IEEE Trans Nucl Sci 1986;NS-33(1):460–3.
14. Wong W, Uribe J, Hicks K, Hu G. An analog decoding BGO block detector using circular photomultipliers. IEEE Trans Nucl Sci 1995;NS-42:1095–101.
15. Adam LE, Zaers H, Ostertag H, Trojan H, Bellemann ME, Brix G. Performance evaluation of the whole-body PET scanner ECAT EXACT HR+ following the IEC standard. IEEE Trans Nucl Sci 1997;NS-44:1172–9.
16. Carrier C, Martel C, Schmitt C, Lecomte R. Design of a high-resolution positron emission tomograph using solid scintillation detectors. IEEE Trans Nucl Sci 1988;NS-35(1):685–90.
17. Huber JS, Moses WW, Derenzo SE, Ho MH, Andreaco MS, Paulus MJ, et al. Characterization of a 64-channel PET detector using photodiodes for crystal identification. IEEE Trans Nucl Sci 1997;NS-44:1197–201.